Medium-scale upper mantle seismic velocity and mass structure below ocean basins

Isabelle Panet[1,2], Marianne Greff-Lefftz[1], Barbara Romanowicz[1,3,4]

[1] Université de Paris, IPGP, CNRS, IGN, Paris ; [2] ENSG-Géomatique, IGN, Marne-la-Vallée ;
[3] Berkeley University ; [4] Collège de France, Paris.

Characterizing the mantle convective flows?

Can we image the Earth's mantle structure at high resolution, and interpret in terms of dynamics?

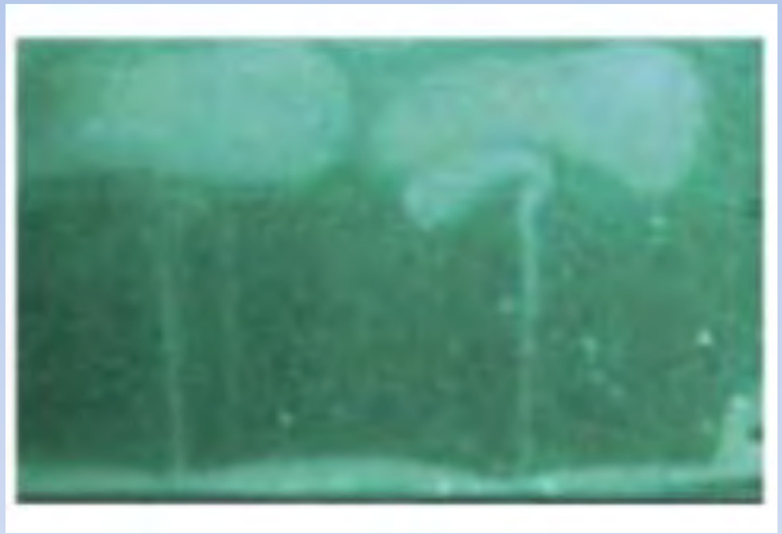

Thin plumes rising vertically in a laboratory experiment (Davaille et al., 2005)

Regular patterns of Rayleigh-Benard convection in a cylindrical container (Bergé & Dubois, 1984)

Decipher different dynamic features, which have been proposed to develop within the Earth's mantle at regional scales.

Medium-scale, regular structures in ocean basins?

Looking inbetween the global convection pattern and
short-scale upper mantle structures in geophysical data

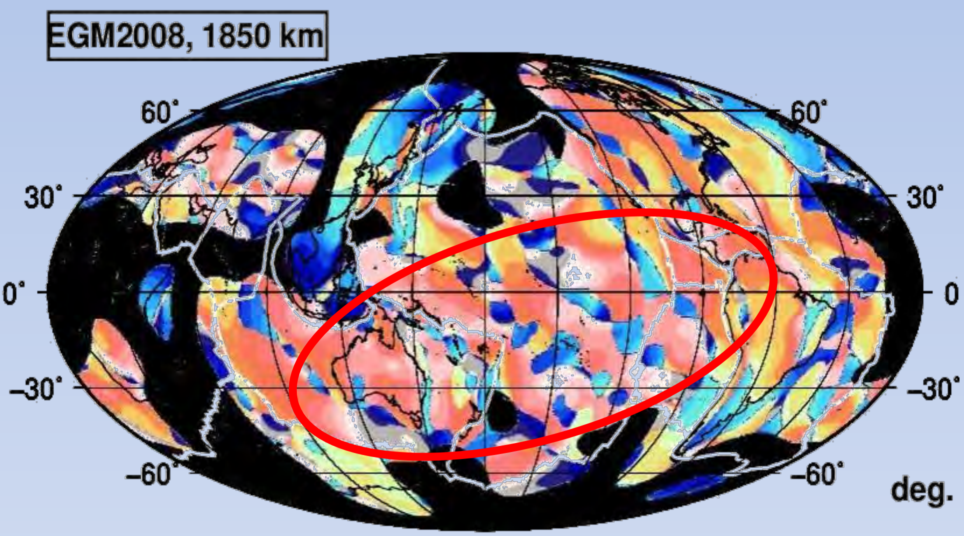

Hayn *et al*. (2012): Existence of a medium-scale **elongated geoid fabric**.

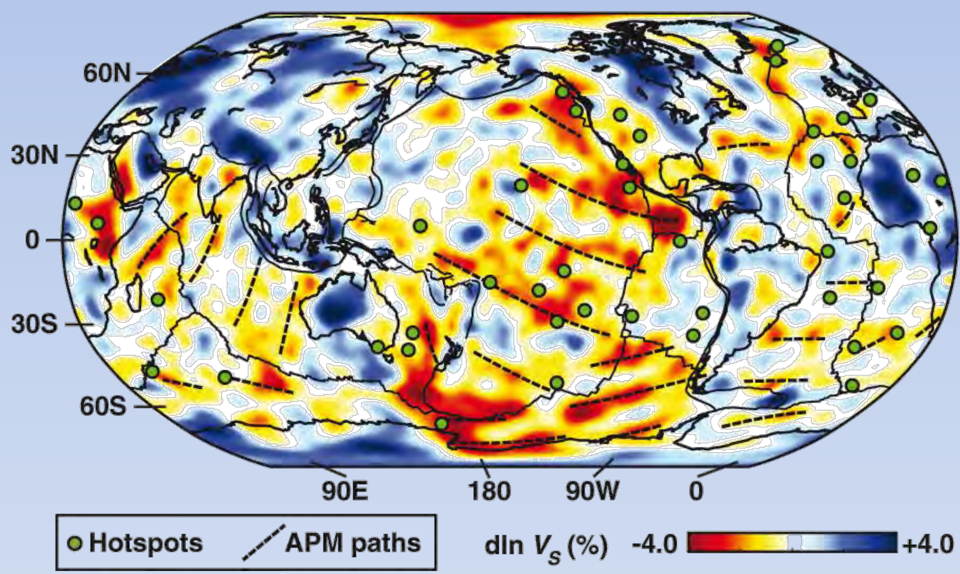

French *et al*. (2013): **Semum2 shear velocity model** at 250 km depth.

*Unexplained **1500-2000 km wavelength seismological anomalies and gravity field structure** along present-day absolute plate motion* (*APM*).

Objectives

Identify and reconstruct elongated, medium-scale gravity and seafloor topography anomalies over ocean basins, for a joint interpretation with seismic tomography

$\rightarrow$ what constraints do we obtain on the regional patterns of the mantle dynamics?

Separate signals at different scales, with different shapes

400 – 4000 km scales

- Extract geoid components at different scales by spherical wavelet filtering,
- At each scale, describe the geometry of the signals by calculating gravity gradients in well oriented frames.
- Same approach applied in 2D to the seafloor topography

Example: rectangular mass excess oriented along azimut α

T: *potential*

$$g_x = \frac{\partial T}{\partial x}$$

$$g_{xx} = \frac{\partial g_x}{\partial x}$$

Gradients scale = source width

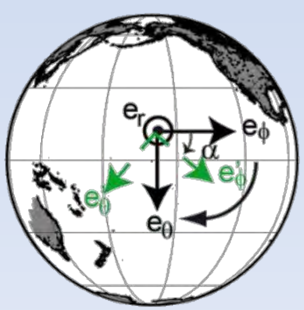

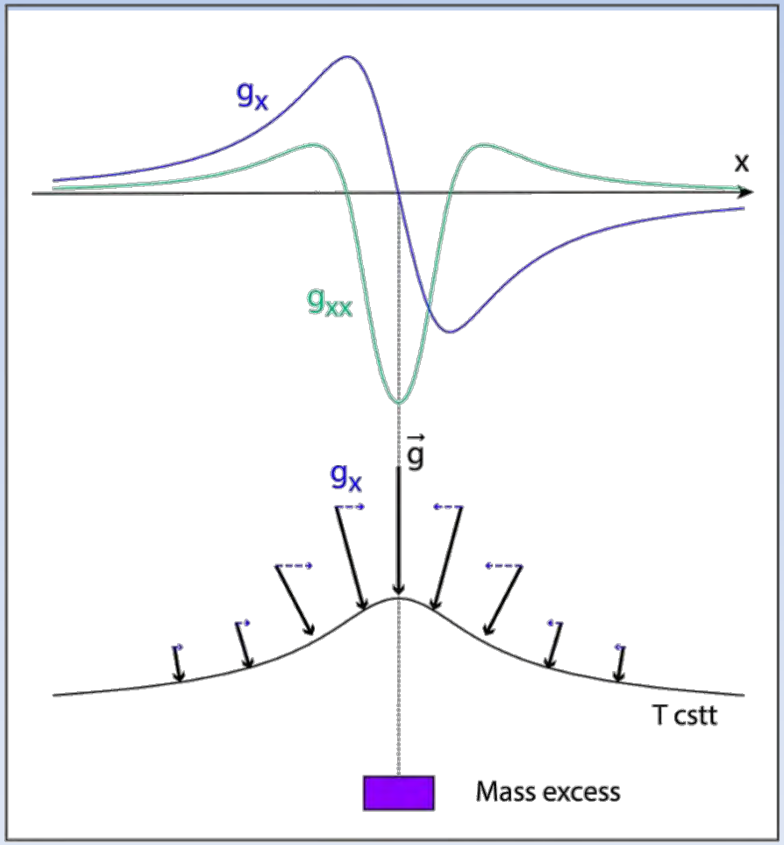

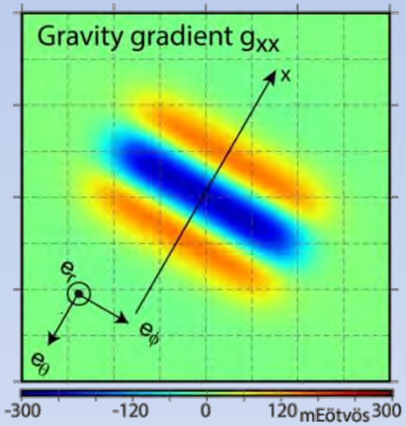

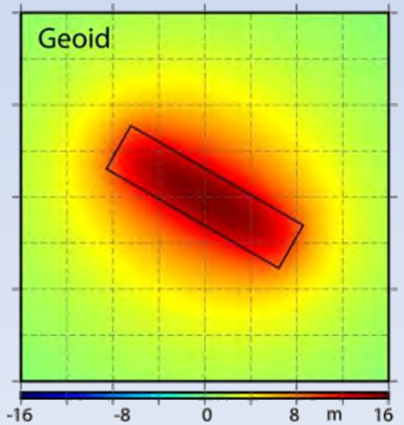

Detection of oriented mass structures by rotation of the spherical frame

Best detection: axes of the frame aligned with the source orientation α_S

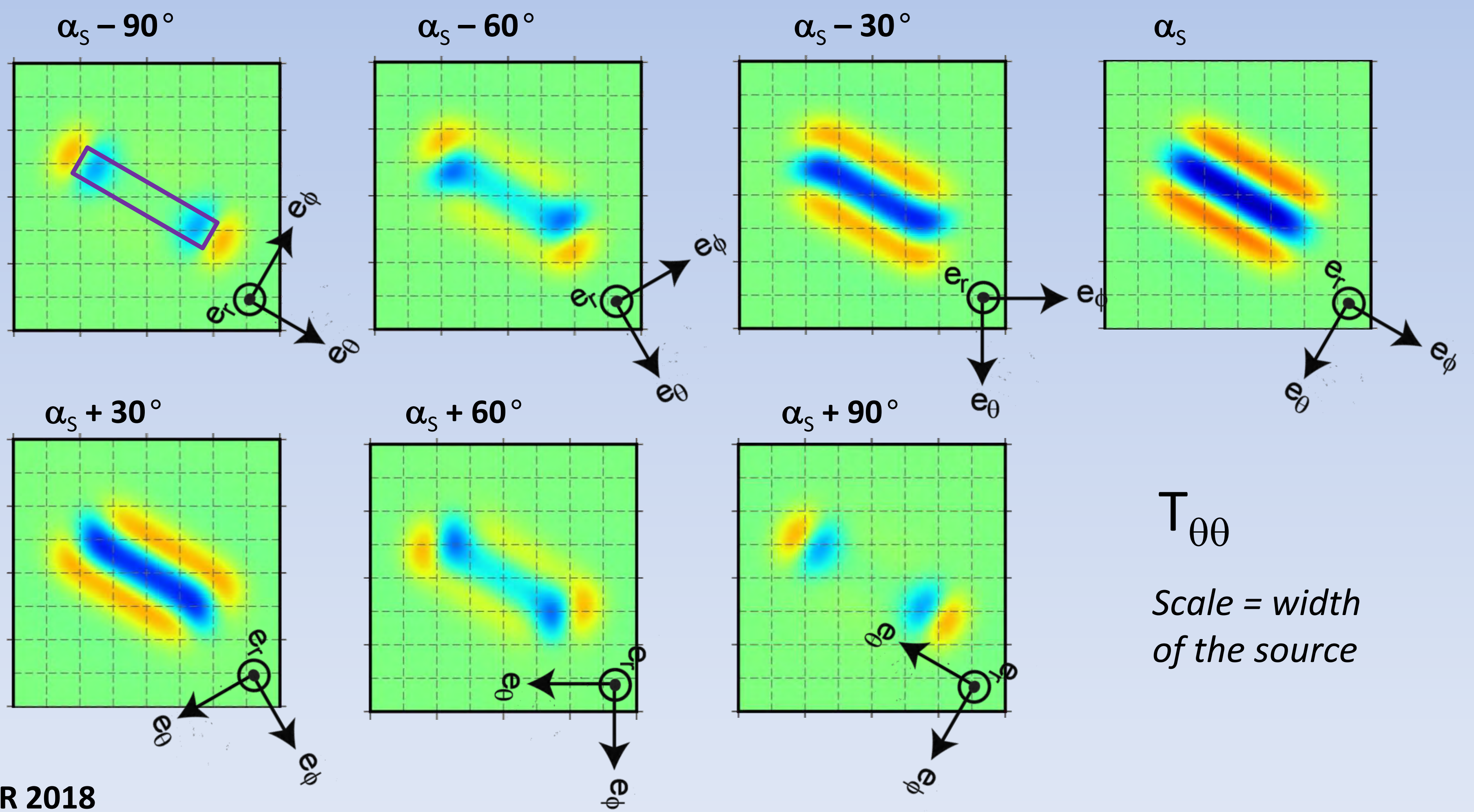

$T_{\theta\theta}$

Scale = width of the source

Panet, JGR 2018

Scale-orientation diagram in the Central Pacific

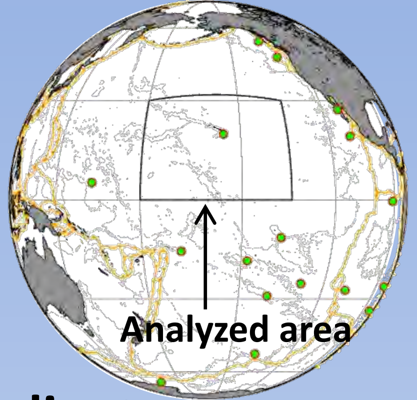

GRACE gravity gradients

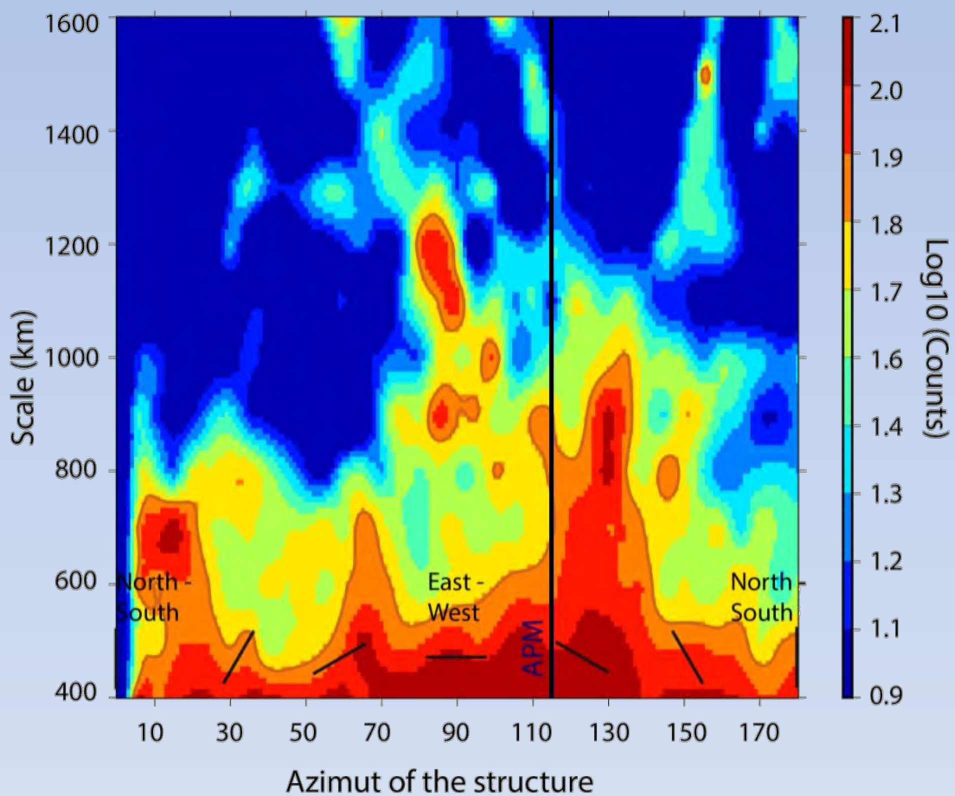

Seafloor slope gradients

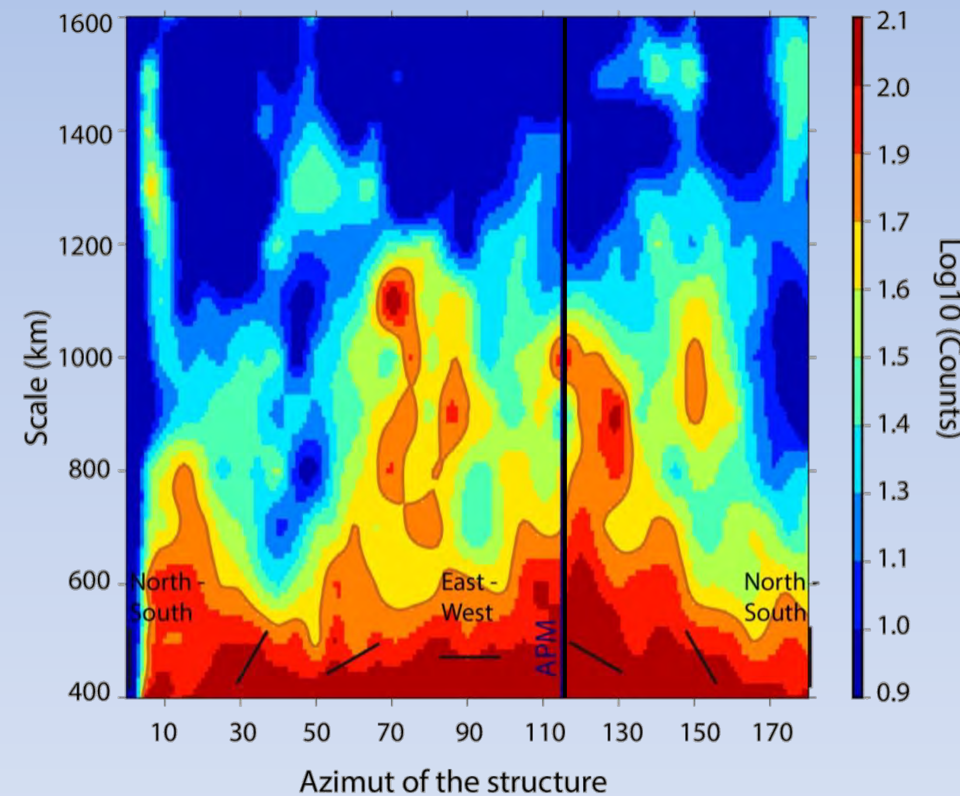

Data: - *GRACE/GOCE global geoid model up to d/o 260* (*Bruisma et al., 2013*)

- *Smith & Sandwell V16.1 bathymetry, corrected from the isostatic contribution of the sediment load* (*Smith & Sandwell, 1997*)

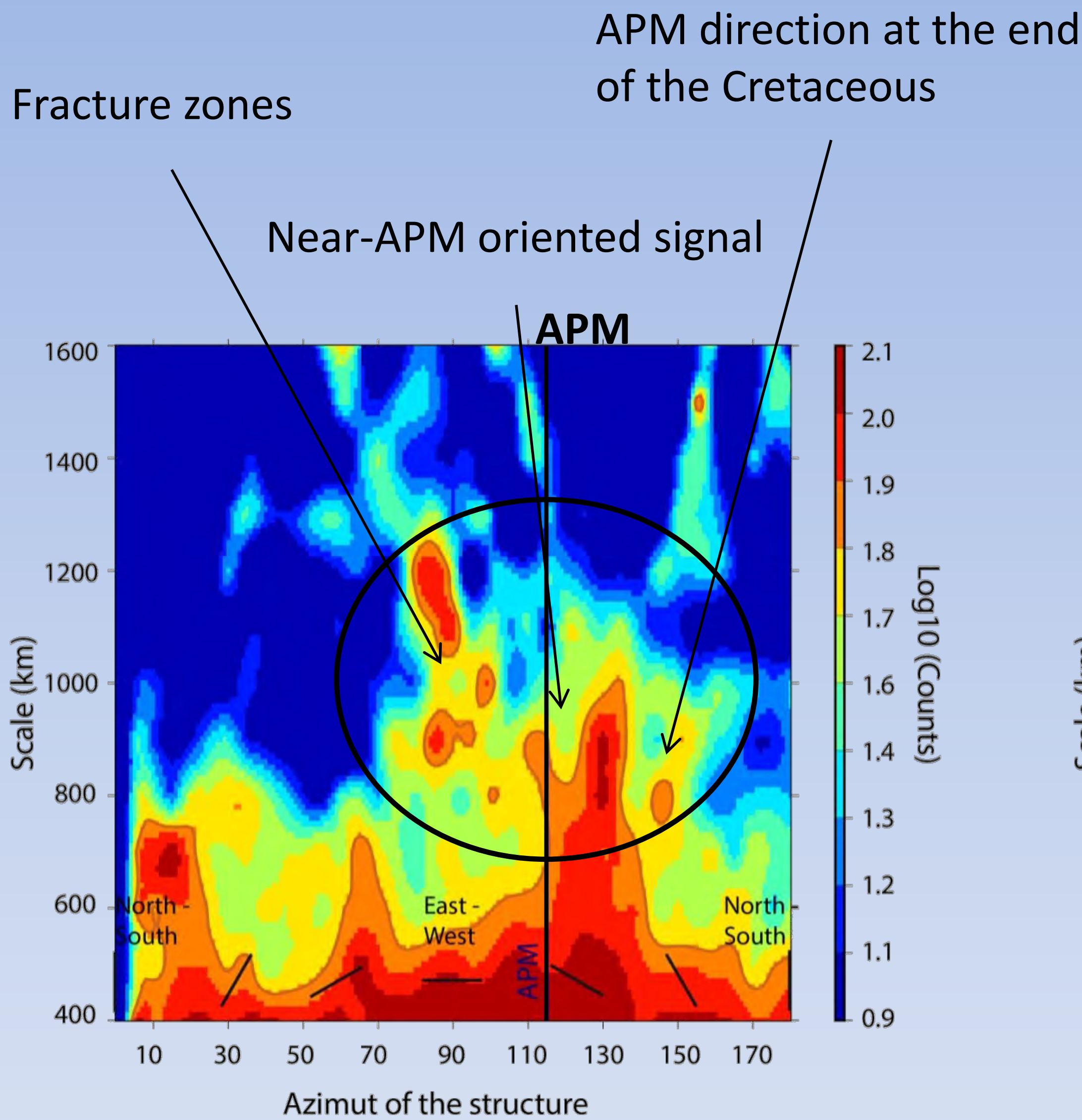

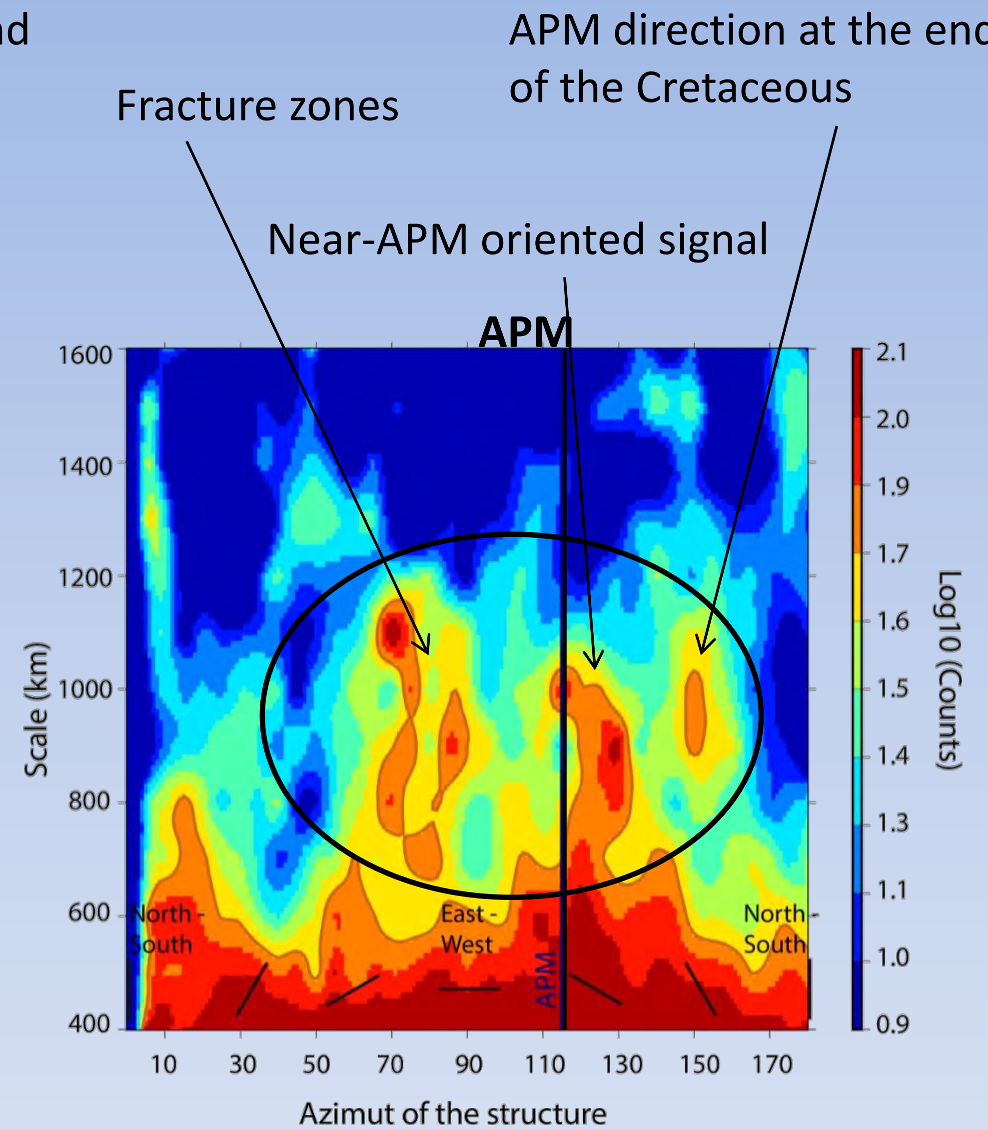

In addition to the smaller-scale signals,

a concentration of energy at intermediate (~800-1200 km) scales

A medium-scale, near-APM oriented periodic signal over the Pacific

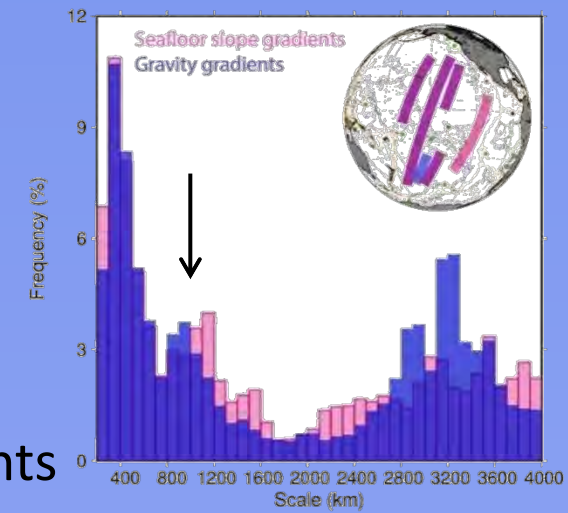

scale = half-wavelength,

histogram for profiles across the undulations

GRACE gravity gradients

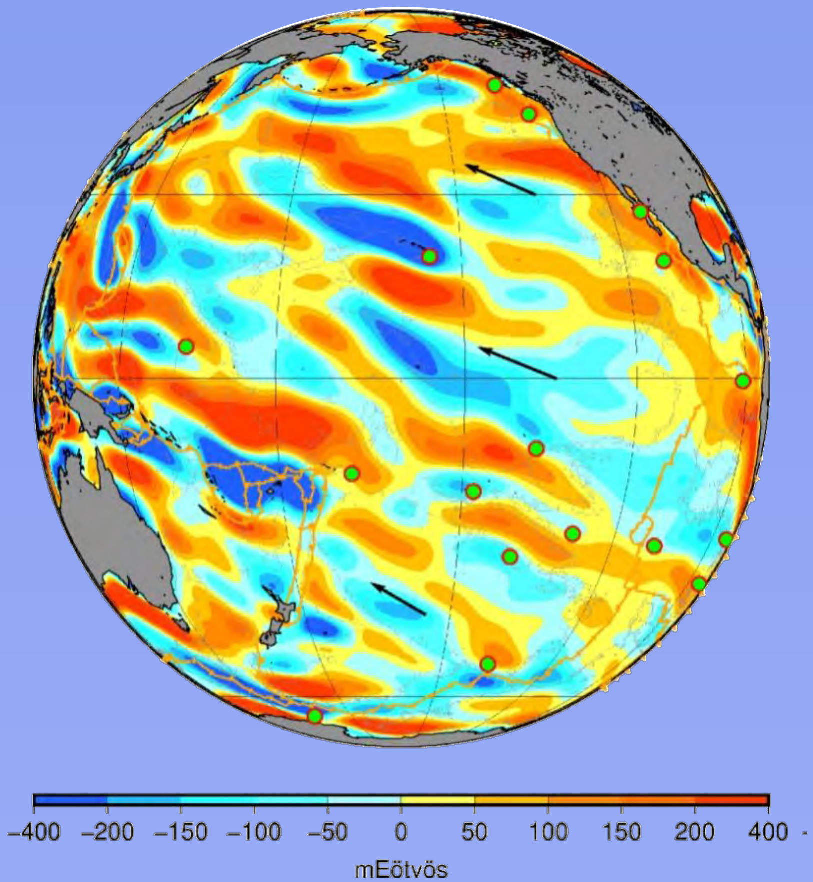

Seafloor slope gradients

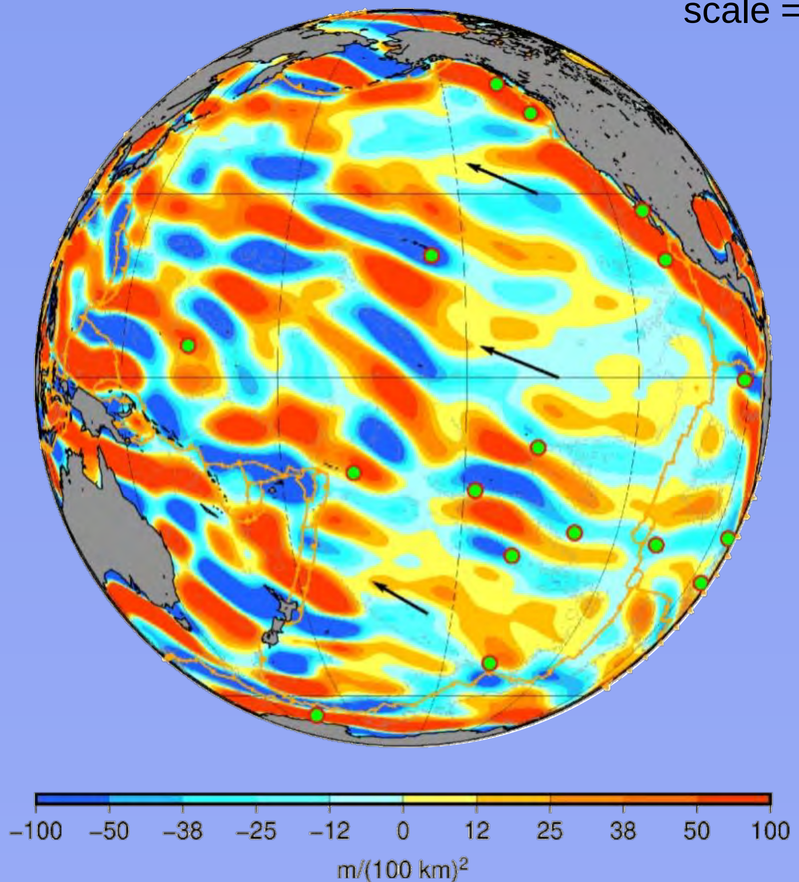

Tθθ
sc. 1100 km
rot. 10-40°

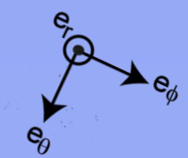

A medium-scale, near-APM oriented periodic signal over the Pacific

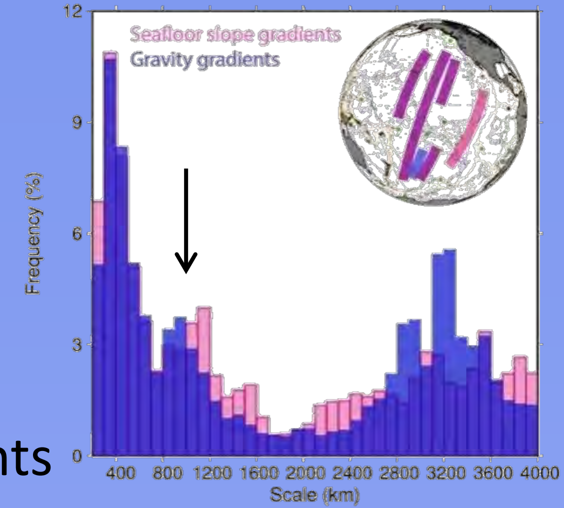

scale = half-wavelength,

histogram for profiles across the undulations

GRACE gravity gradients

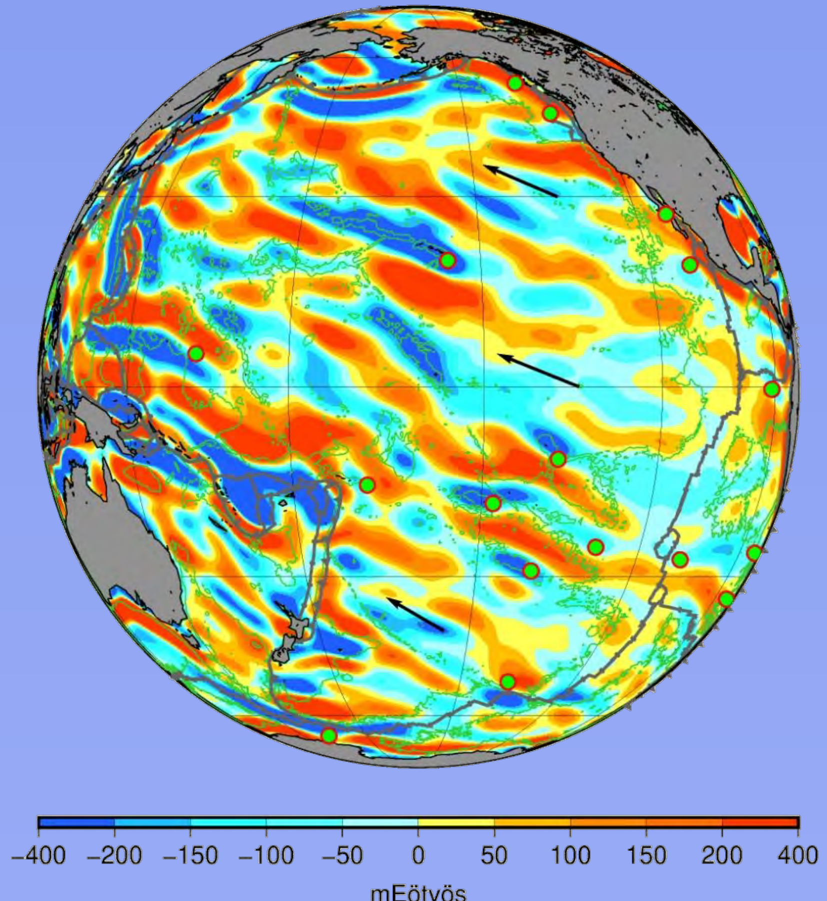

Seafloor slope gradients

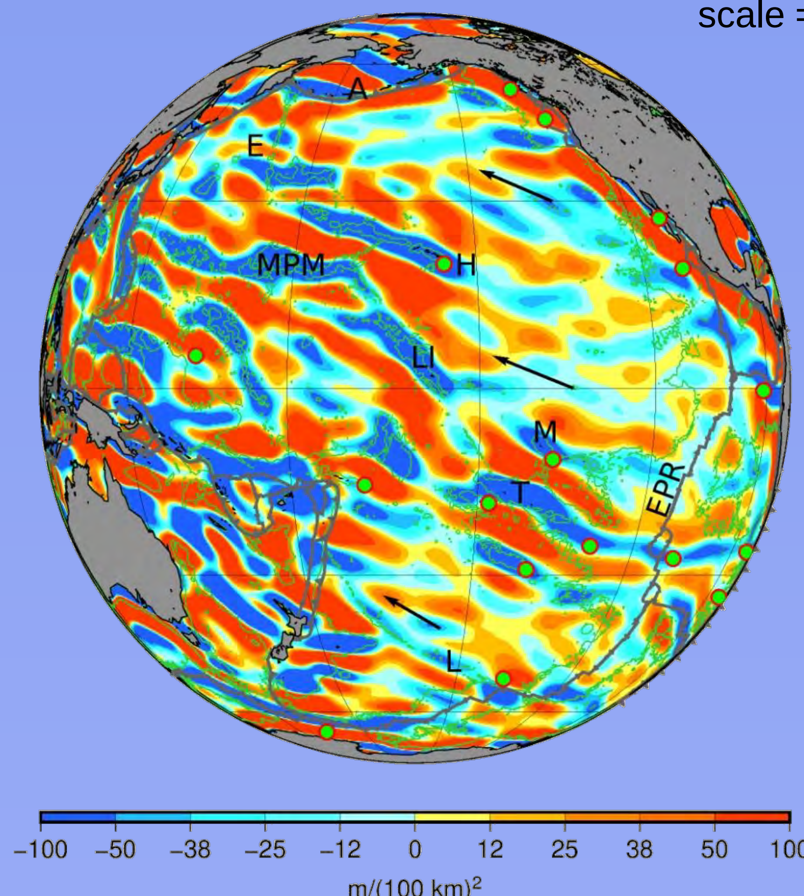

Tθθ
sc. 800 km
rot. 10-40°

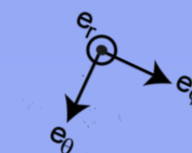

Widespread signals,
also found in other ocean basins

- **Fast-moving** Australian – Indian plates

- **Slow-moving** Antarctic plate

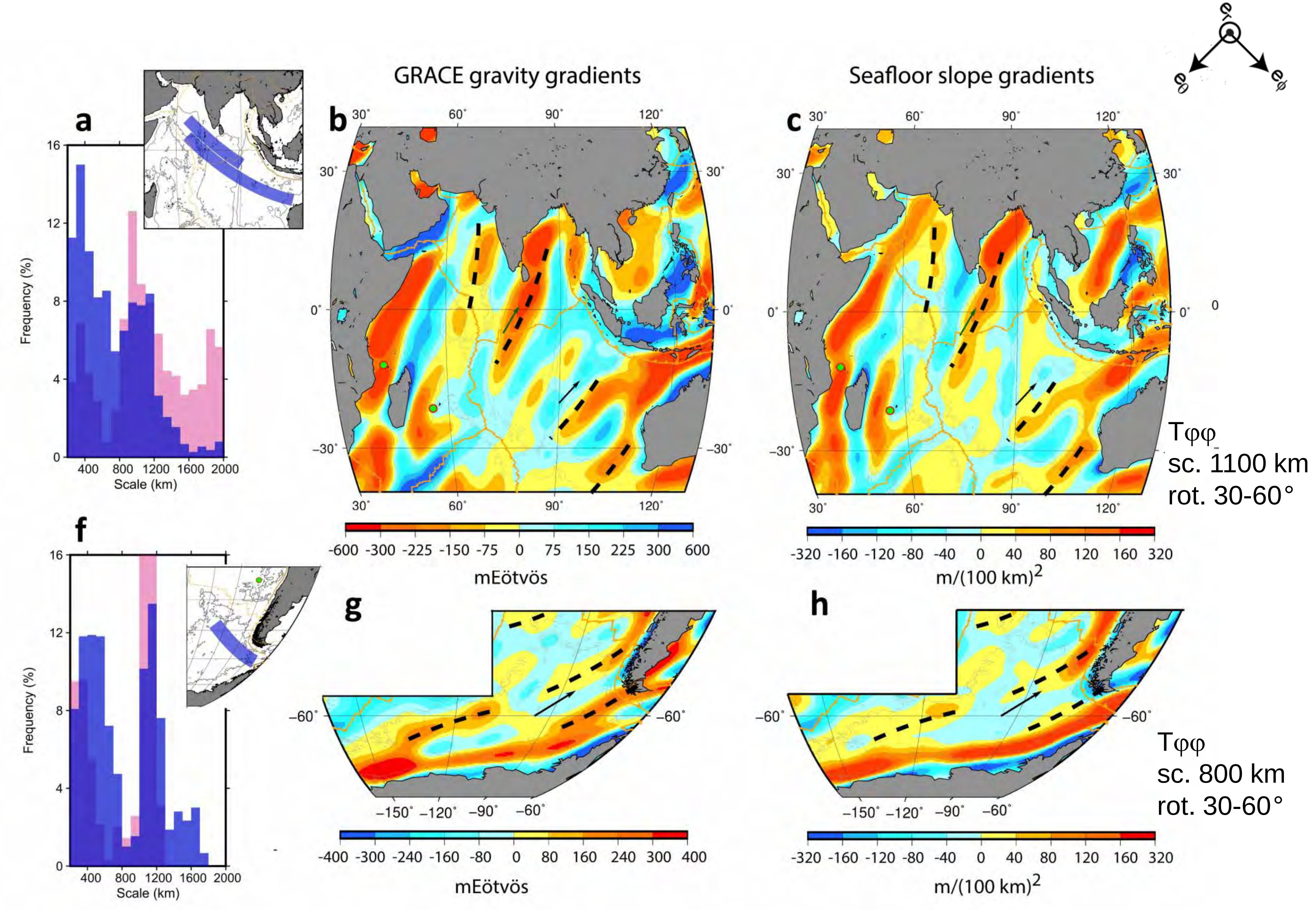

Gradient signals of an equilibrated system of two sources

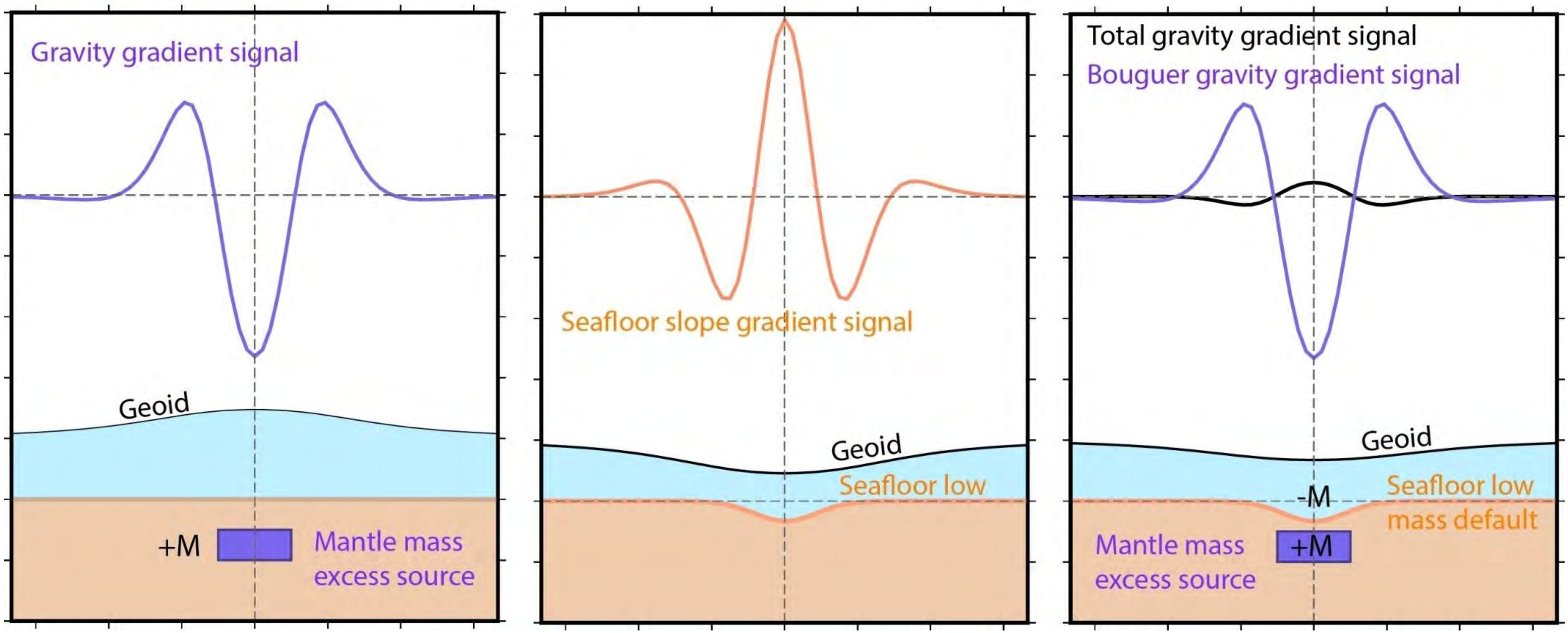

A. Mantle mass excess B. Seafloor low A + B

Removal of the topographic contribution to the observed gravity
→ Bouguer gravity gradients

Comparison with the seismic tomography

- Seafloor lows and mantle mass excess coincide with the slow velocity fingers

GRACE gravity gradients

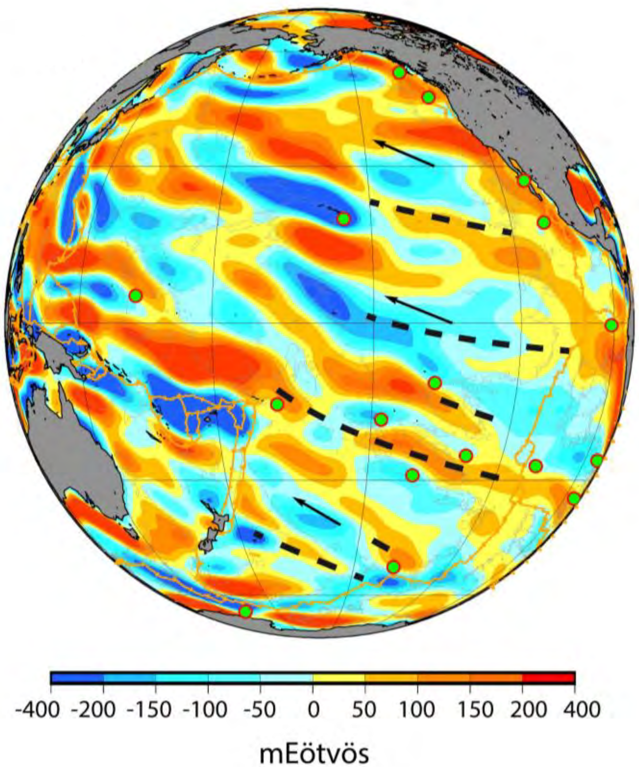

Seafloor slope gradients

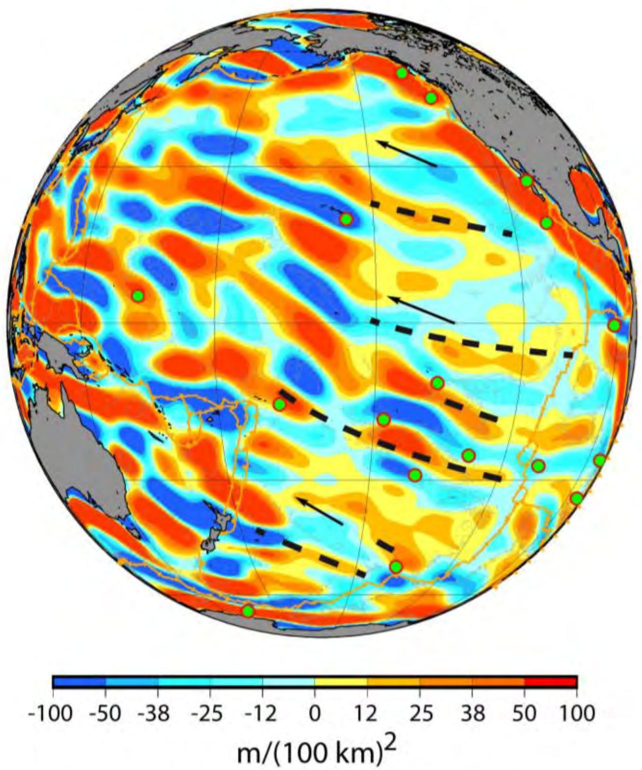

Semum2 model, depth 250 km

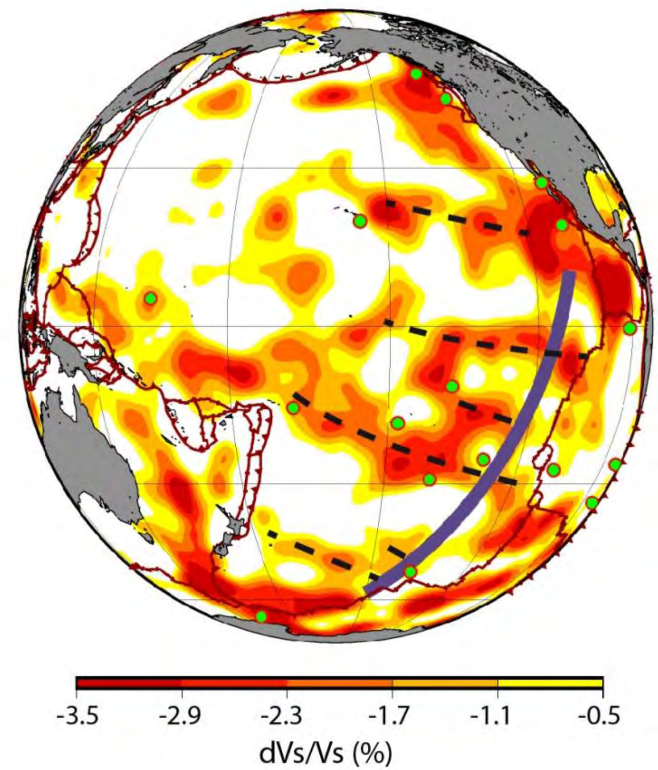

$T\theta\theta$; sc. 1100 km ; rot. 10-40°

French et al. (2013)

Comparison with the seismic tomography

- Seafloor lows and mantle mass excess coincide with the slow velocity fingers

minus Bouguer gravity grads

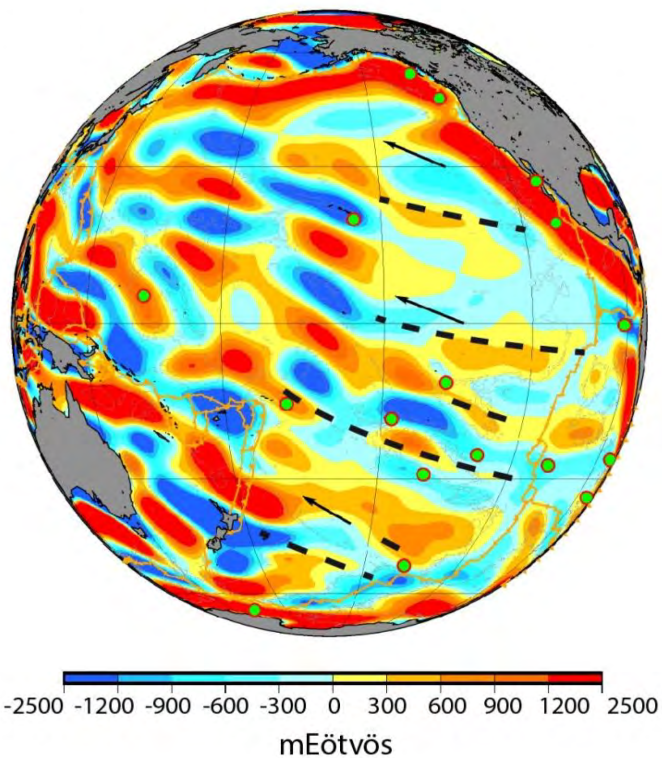

Seafloor slope gradients

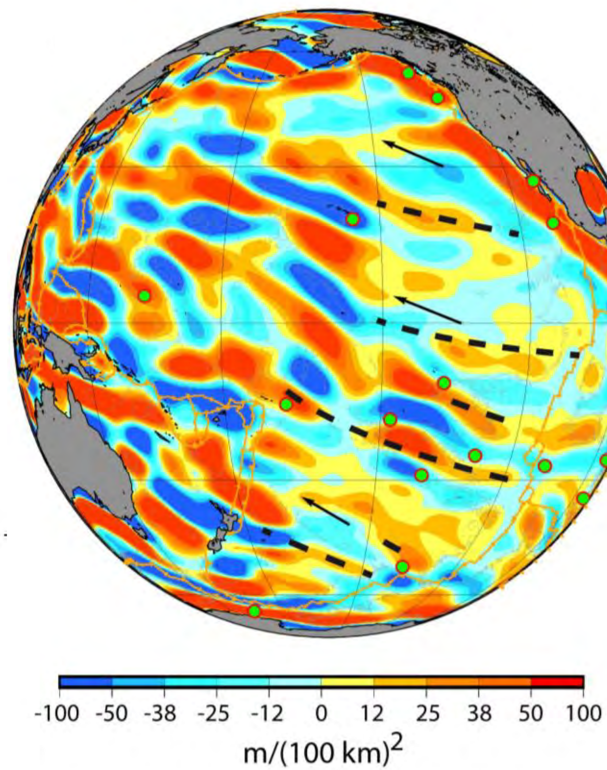

Semum2 model, depth 250 km

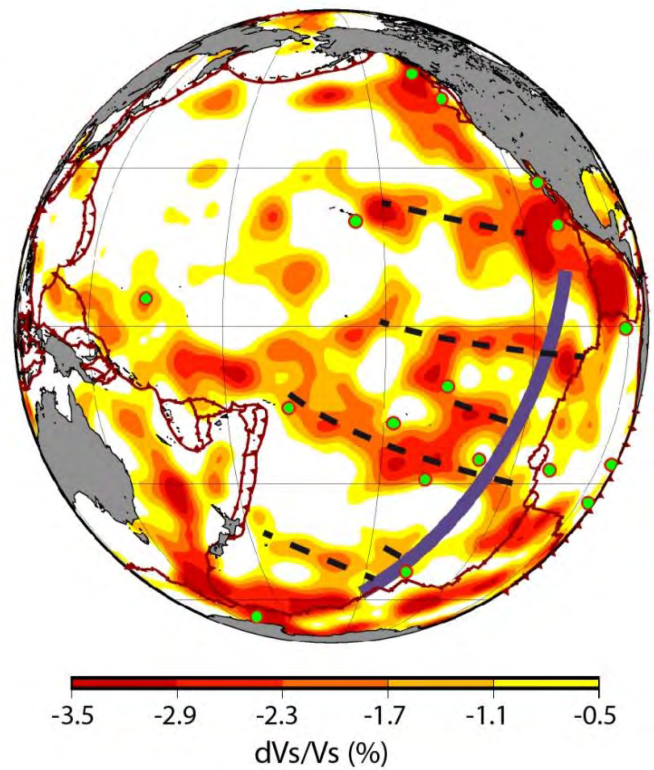

Tθθ ; sc. 1100 km ; rot. 10-40°

French et al. (2013)

Comparison with the seismic tomography

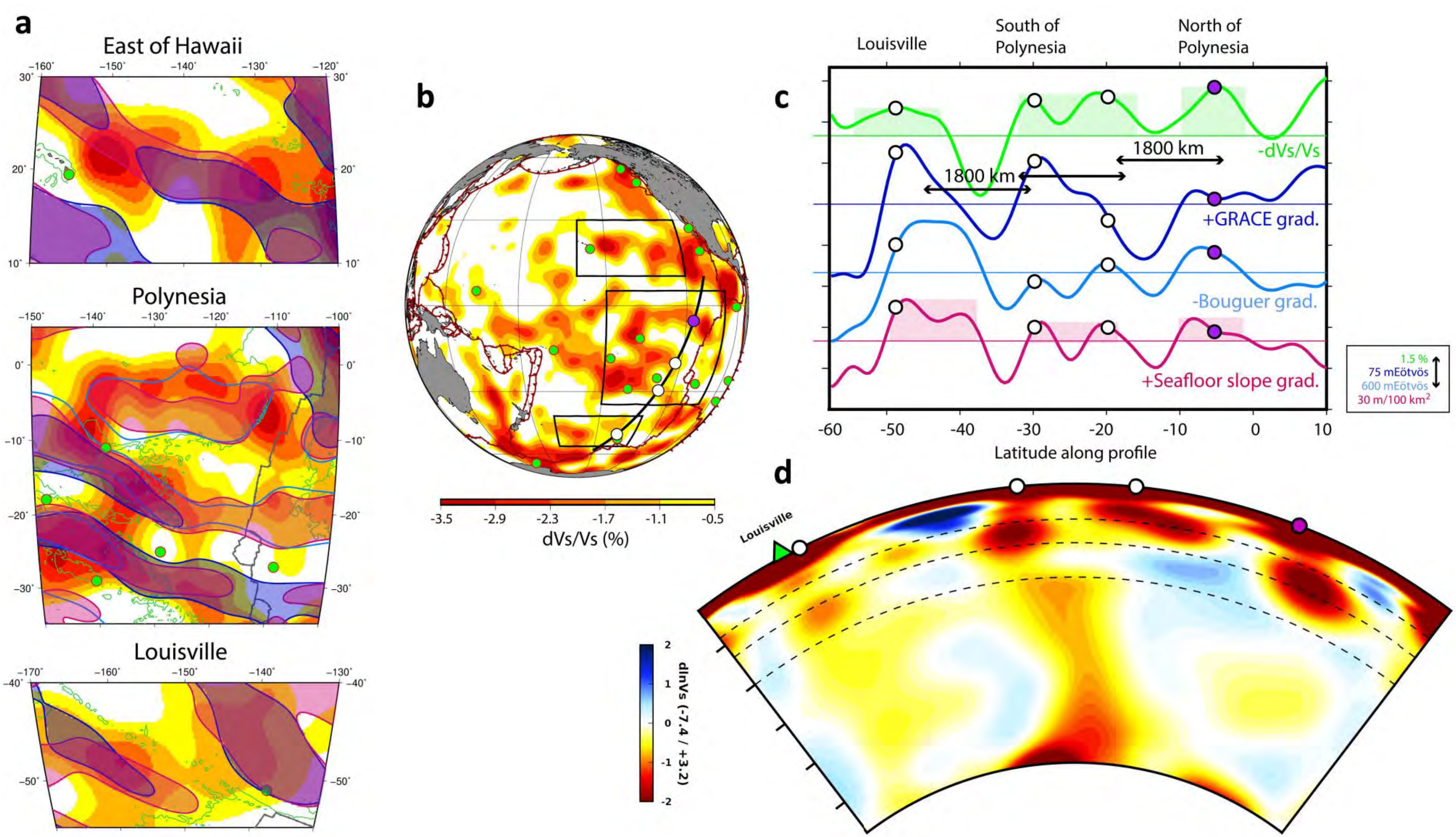

SEMUCB-WM1 (French & Romanowicz, 2015)

Comparison with the seismic tomography

Seafloor lows and mantle mass excess coincide with the slow velocity fingers

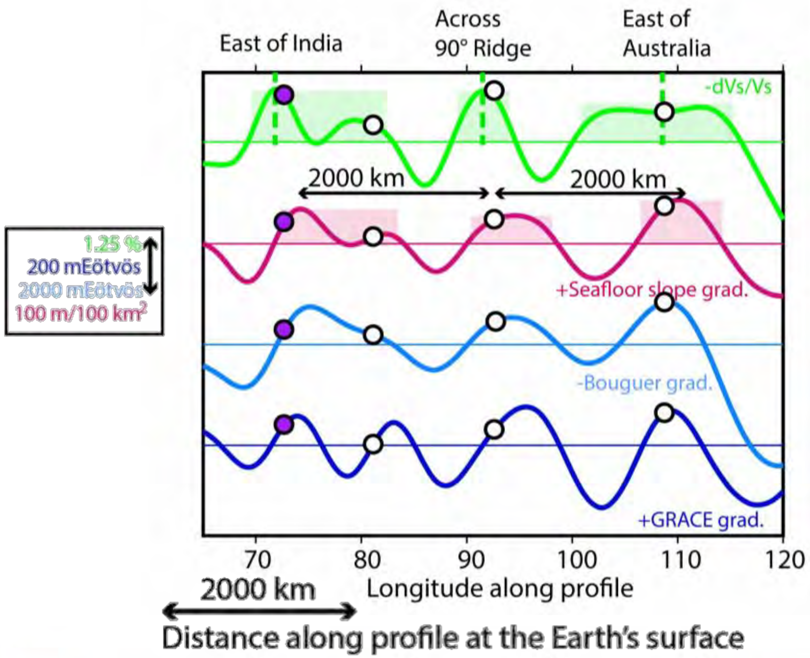

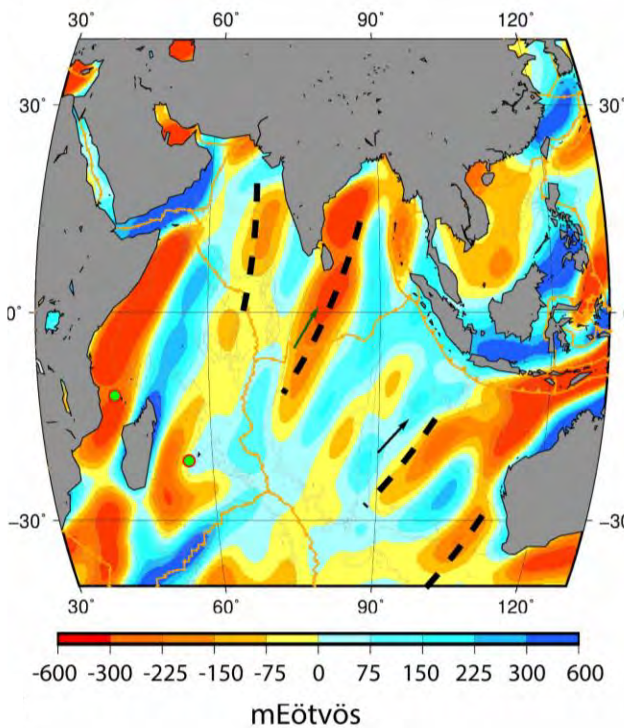

GRACE gravity gradients

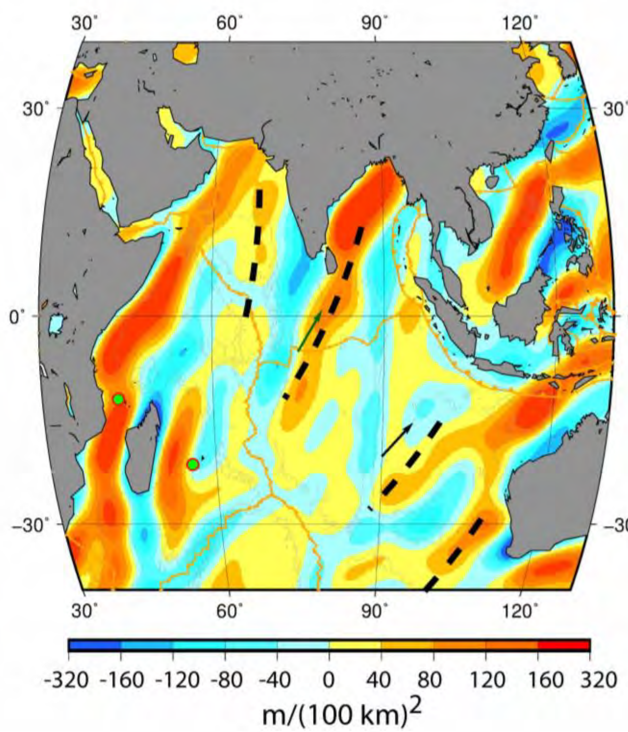

Seafloor slope gradients

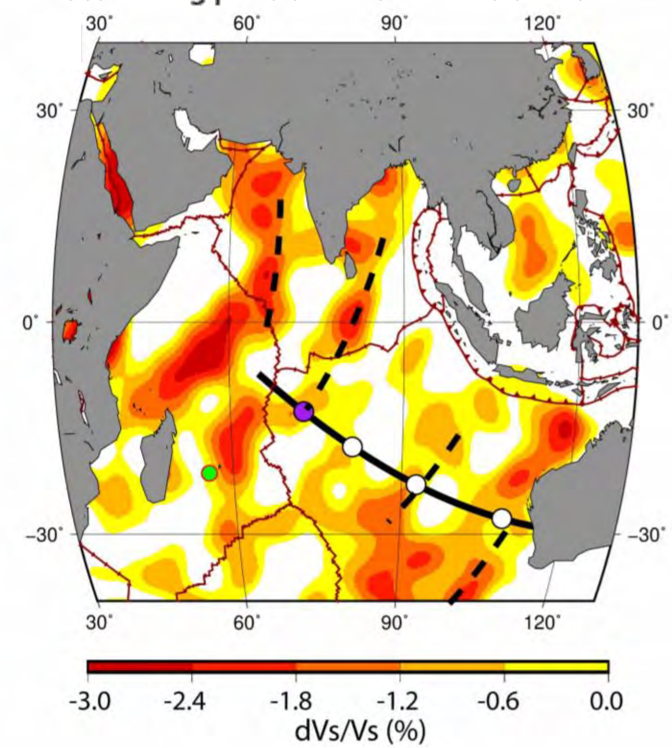

Semum2 model, depth 250 km

Tφφ ; sc. 1100 km ; rot. 30-60°

The Antarctic plate

Consistency with the seismic tomography:

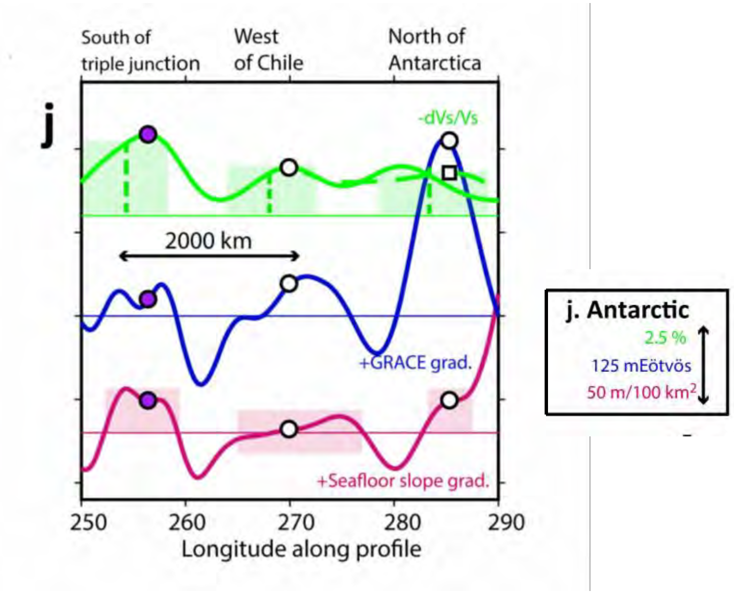

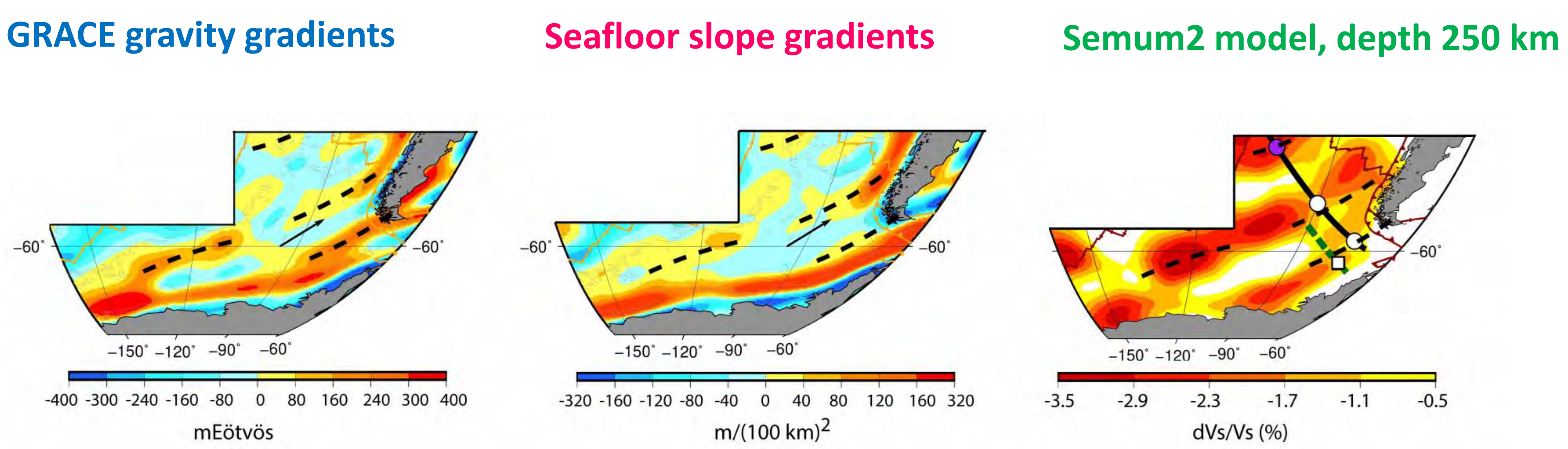

Tφφ ; sc. 800 km ; rot. 30-60°

Comparison with an isostatic crust model

GRACE observed gravity gradients

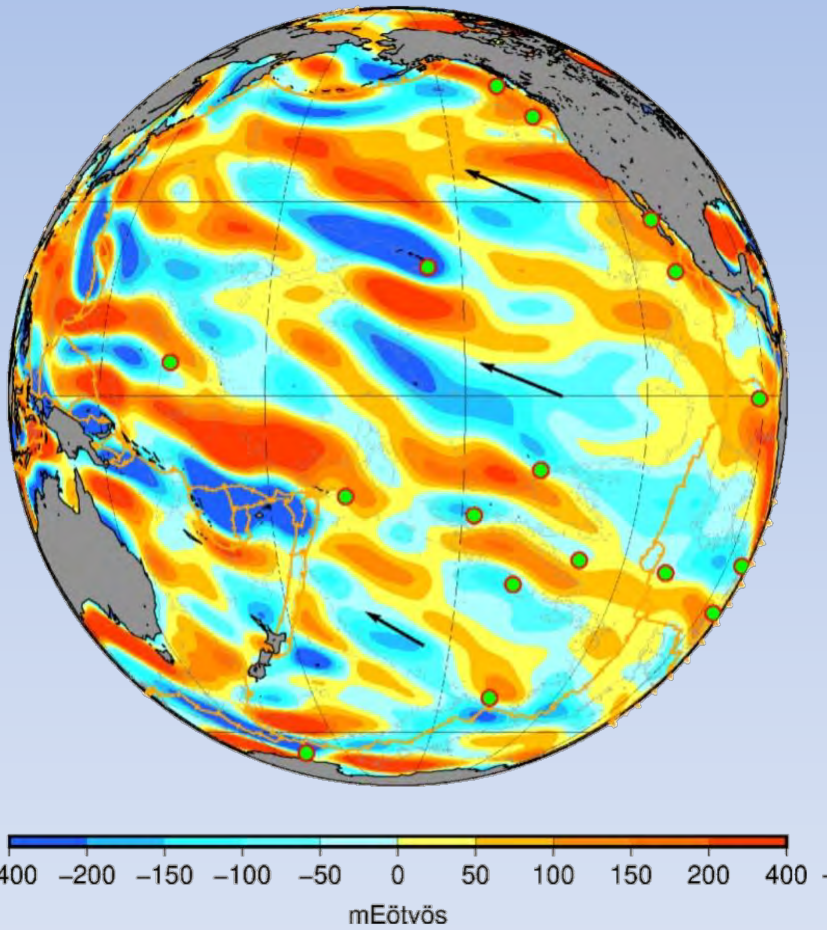

Modelled gravity gradients

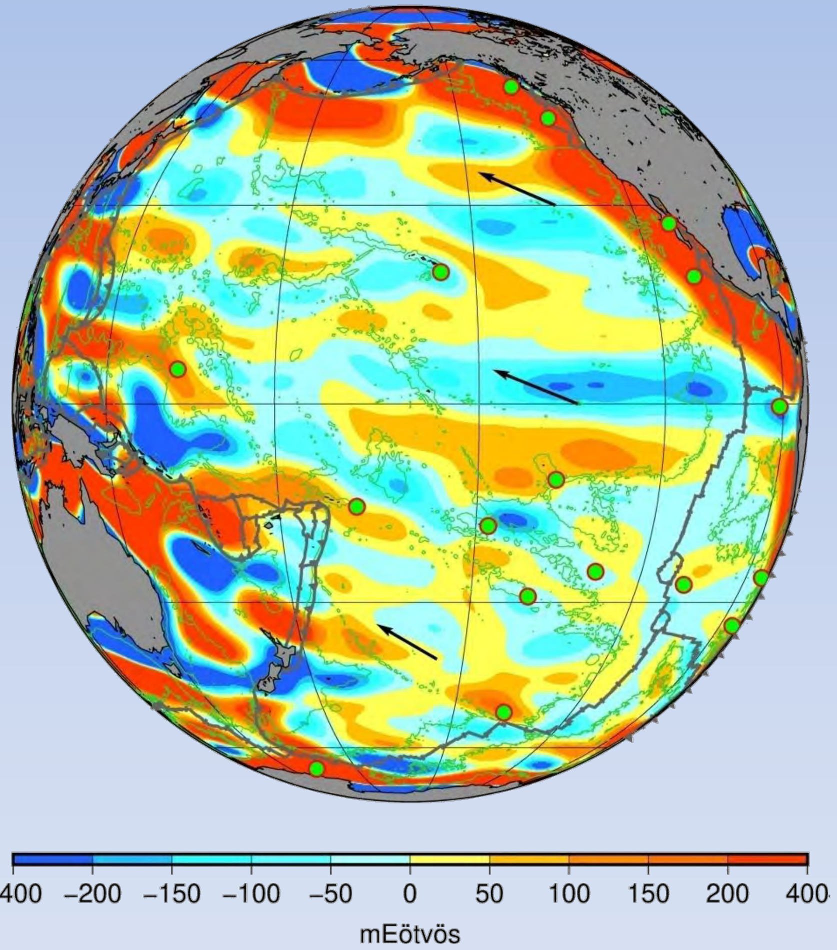

Tθθ
sc. 1100 km
rot. 10-40°

Isostatic crust model including a lithosphere with age-dependent thickness (Conrad & Lithgow-Bertelloni, 2006), following Ricard et al. (2006).

Investigation of crustal models

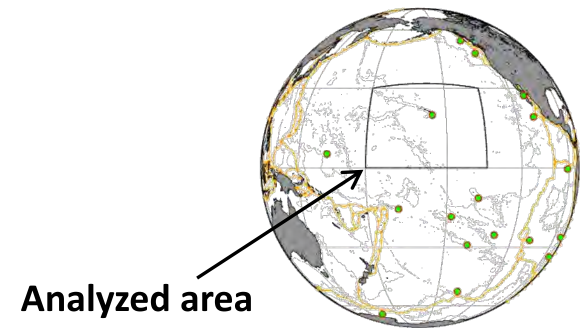

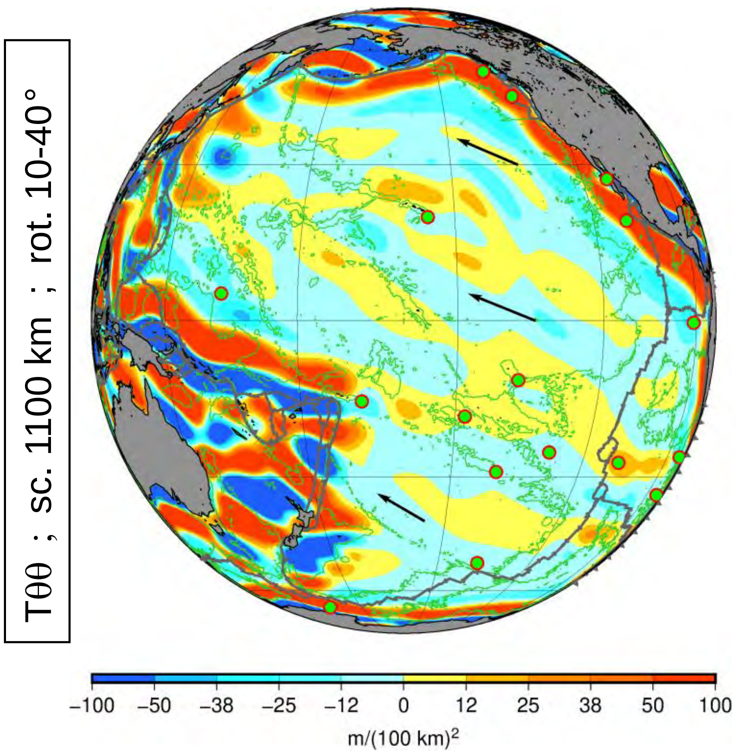

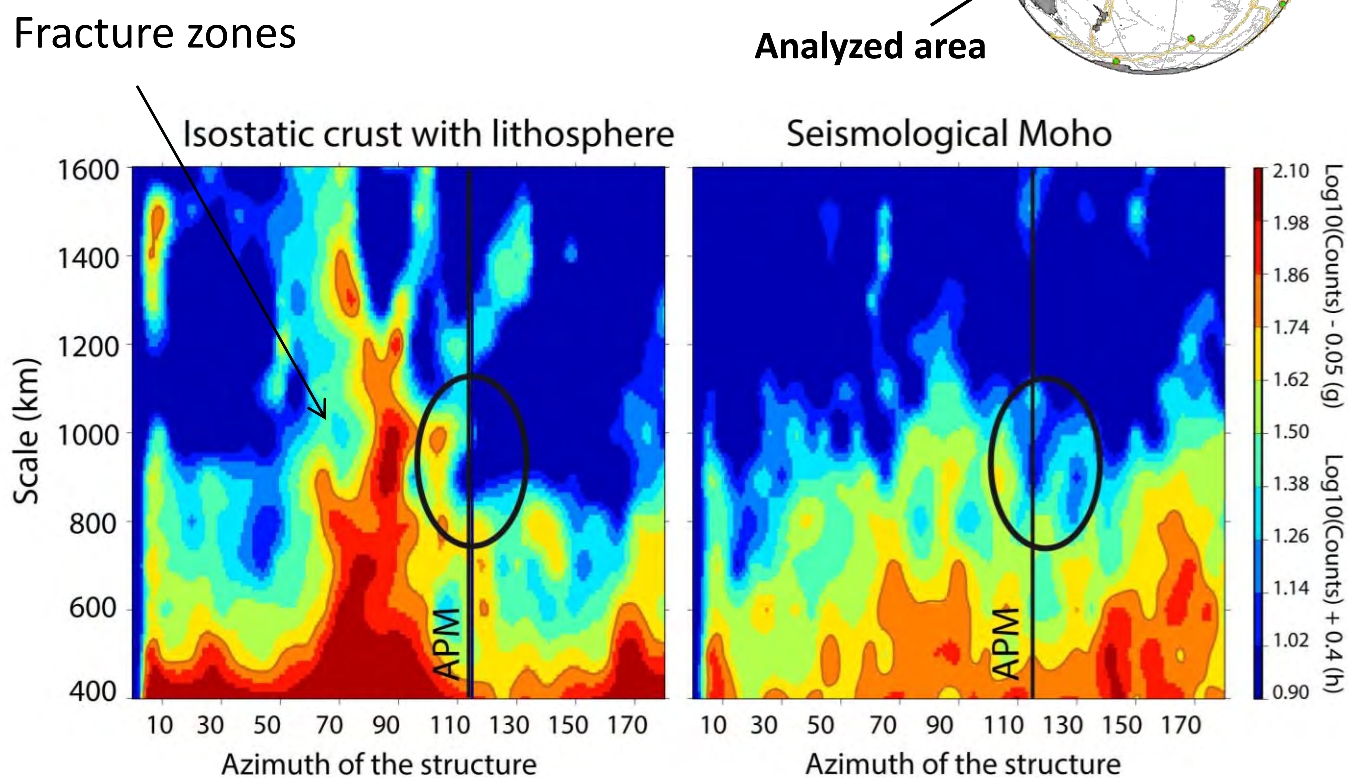

Second-order gradients of the seismic Moho depth by Szwillus et al. (2019), scaled by a factor $\frac{\Delta\rho_{Moho}}{\Delta\rho_{Seafloor}}$: too weak and smooth to explain the data.

No structure along the APM orientation for the isostatic crust model and the LITHO1.0 (Pasyanos et al., 2014) Moho depth map.

Spatial structure of a mantle source?

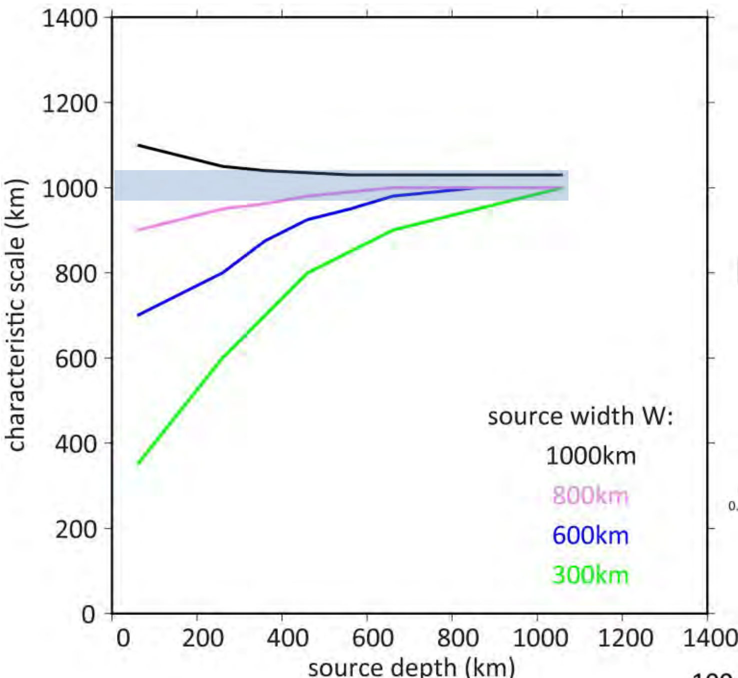

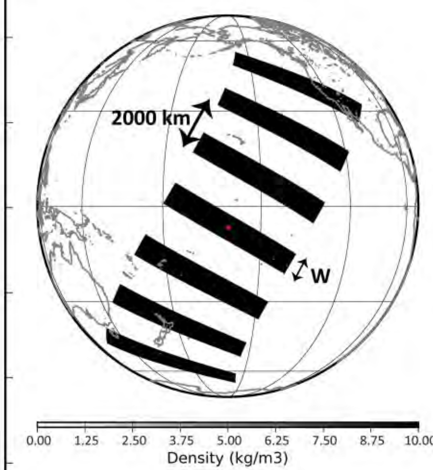

Observational constraints on the spatial structure of the sources:

Width *w* at upper mantle depth and 2000-km period:

scale of a periodic gravity signal

Depth range:

seismic tomography

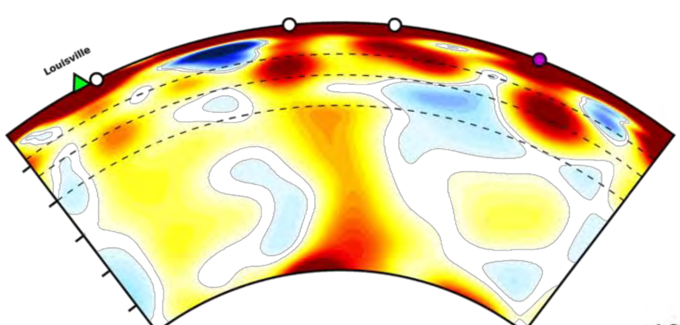

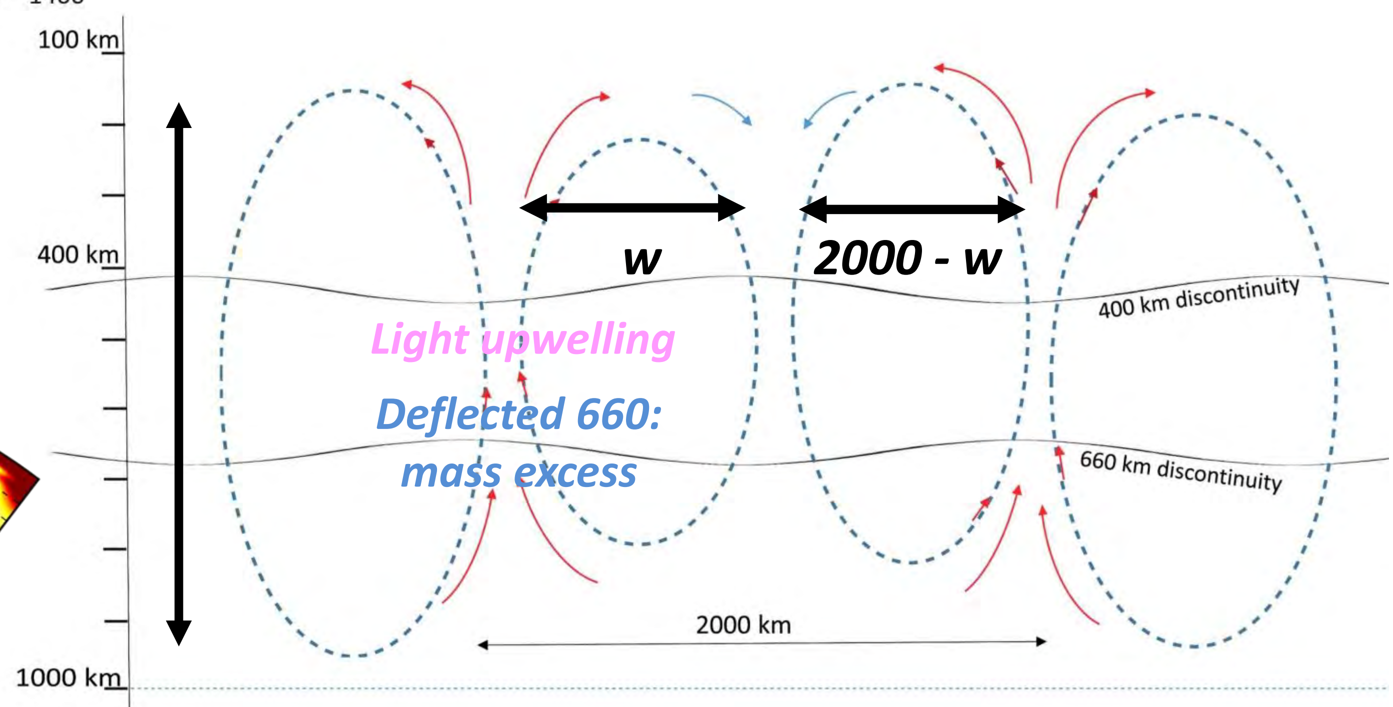

Bi-dimensional Rayleigh-Bénard convection?

Thermal interpretation of the seismic velocity anomalies

• Extended transition zone down to 1000-1200 km depth + 1:1 aspect ratio of the convective cells: a process able to explain the observations geometry

Model	Fit to the Bouguer gravity	Fit to the seafloor topography
Rayleigh-Bénard rolls. Depths: 170-1000 km or 380-1220 km ; ΔT: ±75-200K.	**No** (hot upwelling mass default predominant where mass excess is needed)	**No** (opposite sign)
Rolls with enhanced 660km interface deflection (ringwoodite phase transition) Factor 2 enhancement Factor 8 enhancement	 **No** **Yes** but dynamical problem	 **No** (opposite sign) **No** (opposite sign)
Rolls with shallow decompression melting and lithosphere underplating With or without a factor 2 enhancement of the 660km deflection	**No** (far too large underplated mass: 100-km thick layer with $\Delta\rho$ = 400 kg/m^3 for ΔT = ±100K)	**No** – *and no joint fit of the gravity and topography data*

Mass excess within the hot upwellings?

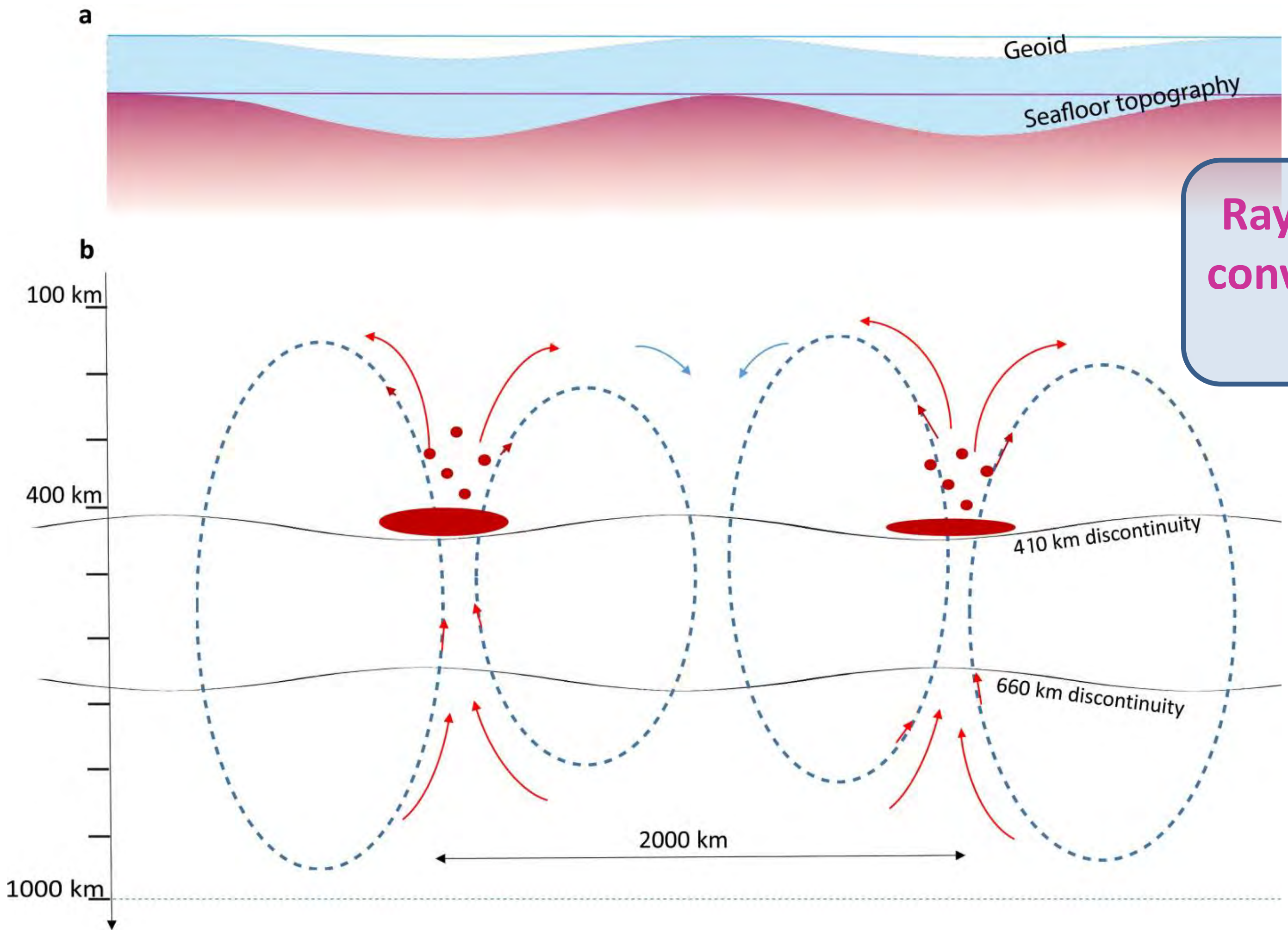

Rayleigh-Bénard style convection with partial melting?

Partial melting when the hot upwellings cross the 410-km wadsleyite phase transition, for a moderately hydrous transition zone (*Bercovici & Karato, 2003*).

→ *Dense, Fe-enriched hydrous melts and cristallized olivine in the upper mantle.*

Mass excess within the hot upwellings?

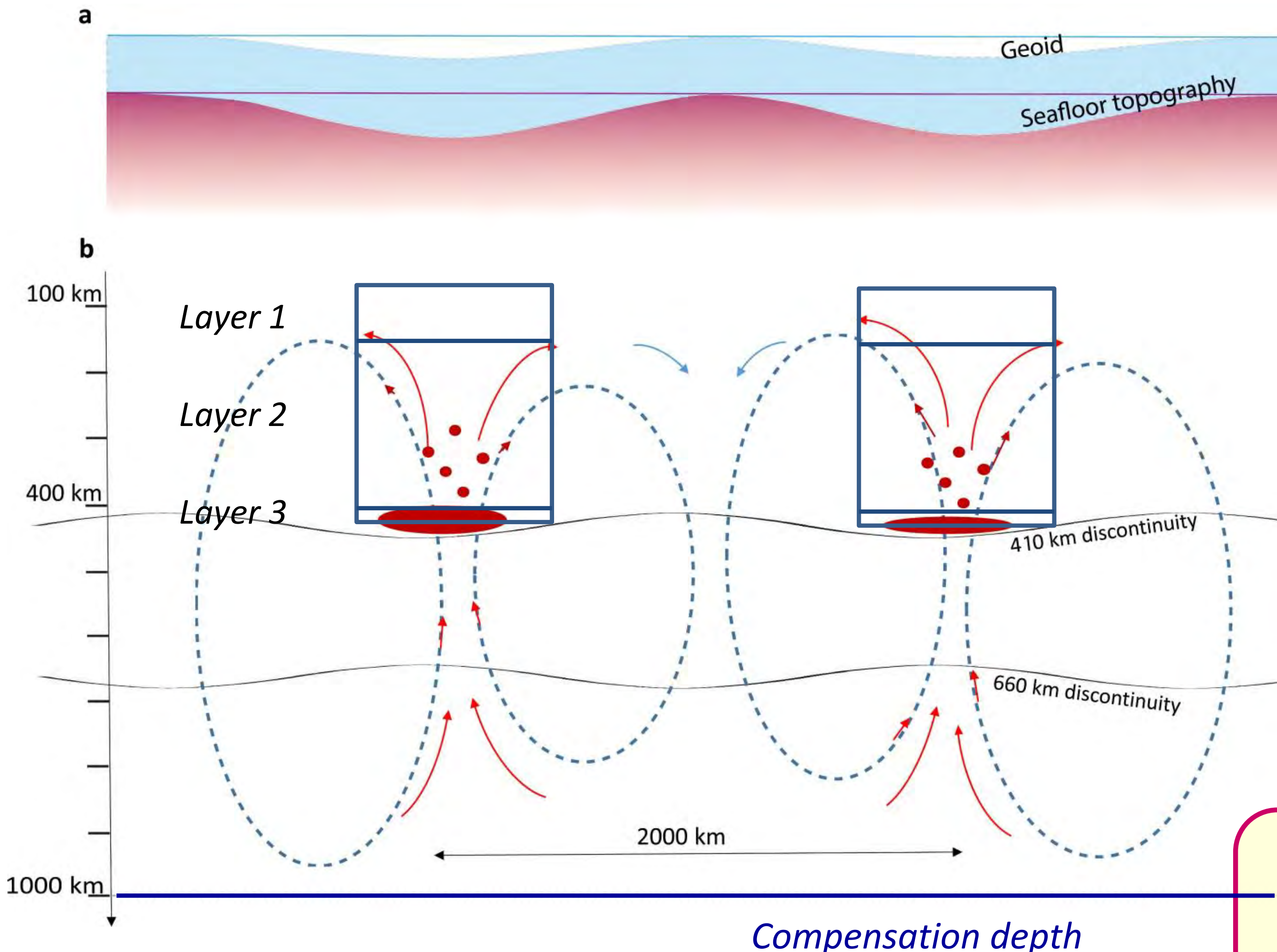

- *Rolls depths:*

  160 – 1000 km
  380 – 1220 km

Deep isostasy
(decorrelation of seismic structure above/below 1000 km depth, Rudolph et al. 2015)

- ***Three layers***: *- 1: sublithospheric (60 – 160 km = the low velocity zone),*
  - 2: underlying upper mantle (160 – 380 km),
  - 3: above the transition zone (380 – 410 km = where a melt layer is proposed based on seismic tomography results).

Effect of a sublithospheric low viscosity layer

Cumulative misfit on the Bouguer gravity gradients, the seafloor slope gradients and the vertical equilibrium (2.5% isolines up to 30% of residual rms)

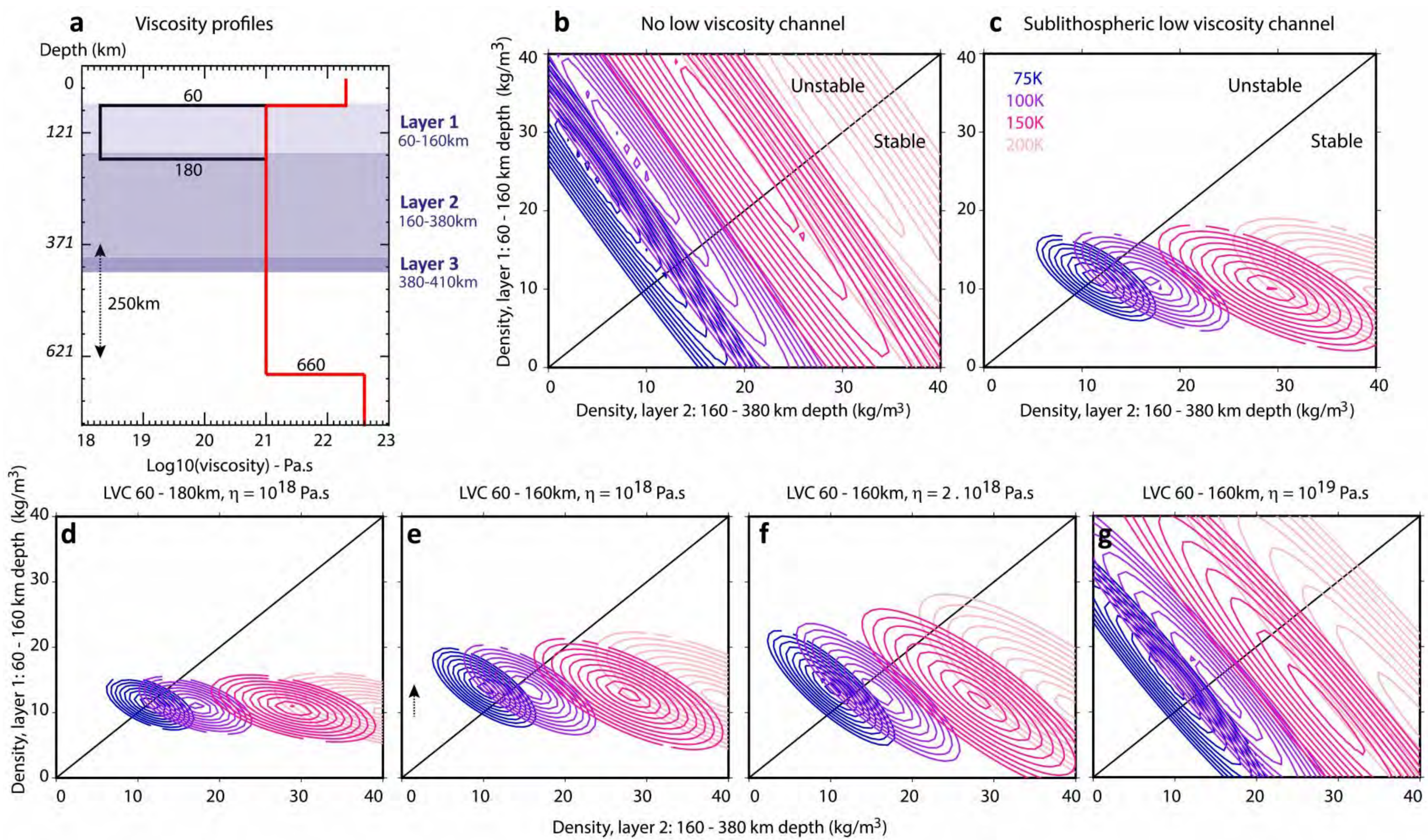

Density anomalies: thermal + compositional

Layer 3: 10 kg/m^3

Acceptable models

Trade-offs between density anomalies in layers 1 and 2

Rolls thermal anomaly:

75K
100K
150K
200K

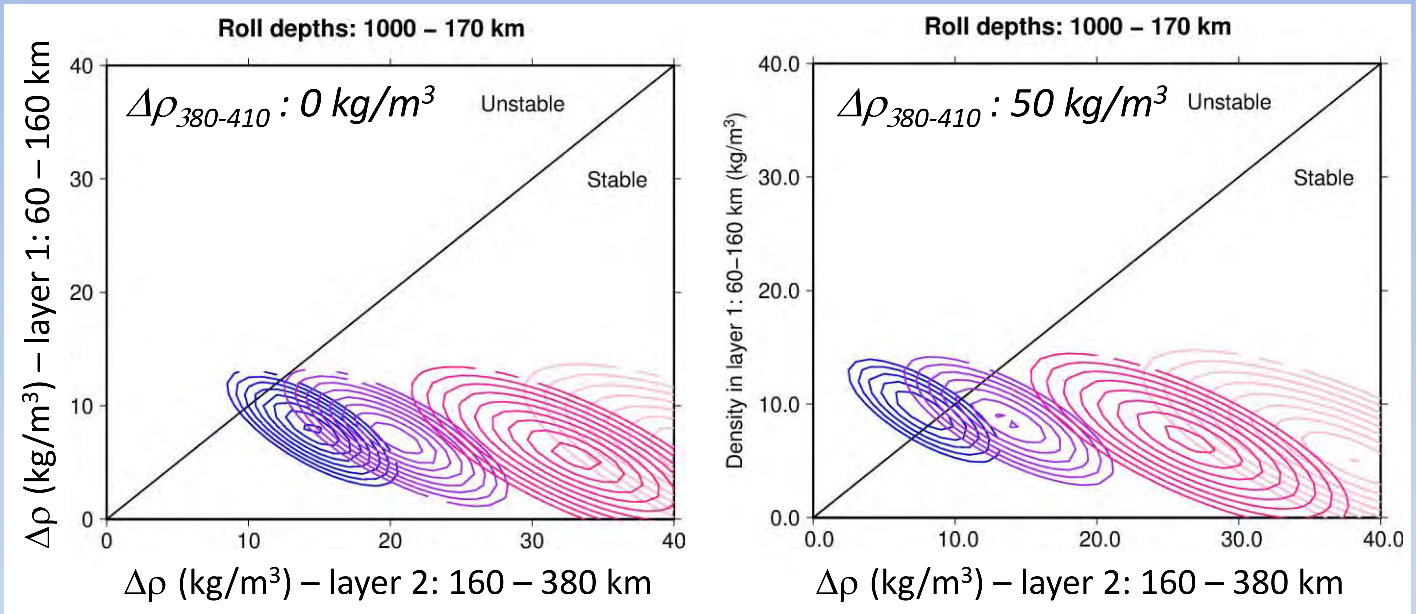

- ***Low viscosity channel*** $\rightarrow$ *mass in the sublithospheric layer well constrained from topography ; stable layer with respect to the underlying mantle.*

- *No (stable) solution without mass excess in layer 2*

  $\rightarrow$ ***mass excess across all three layers****.*

- *Melt fractions < 1 wt% $\rightarrow$ mass excess mainly in the cristallized olivine:*

  1% Fe-enrichment with respect to Mg: $\Delta\rho$ = 15 kg/m^3

Conclusion

• We identify a **regular pattern of near APM-oriented, ~2000 km wavelength undulations in GRACE gravity and seafloor topography** over wide ocean basins.

Seafloor lows and mantle mass excess coincide with slow upper mantle seismic velocity fingers (Semum2 model).

• The observations geometry can be explained by deep Rayleigh-Bénard type convection down to the base of an extended transition zone.

• **The flow may not be entirely driven by plate motions as for Richter rolls**: signals are observed beneath both fast- and slow-moving (Antarctic) plates.

• **The mass excess and seafloor lows likely reflect dense sources in hot upwelling areas, across the upper mantle.**

Possible origin related to the formation of dense melts as the rolls cross a moderately hydrous transition zone. Acceptable models require a low viscosity zone below the lithosphere.

Supplements

The Tonga-Hawaii profile

- Along a profile between Tonga and Hawaii: fast upper mantle seismic velocities coincide with geoid and topographic highs.

Periodicity ~1500 km.

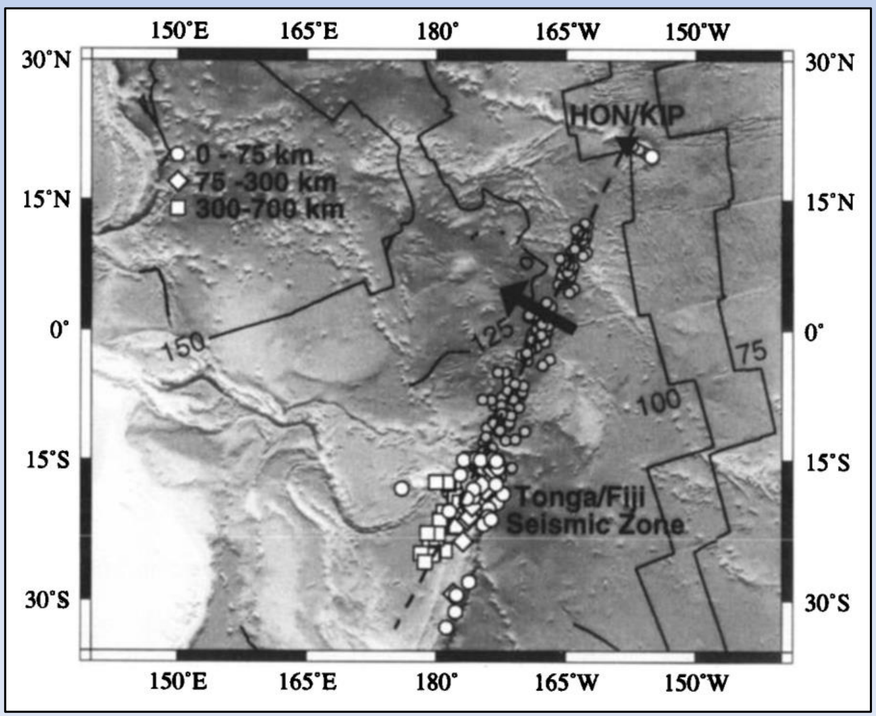

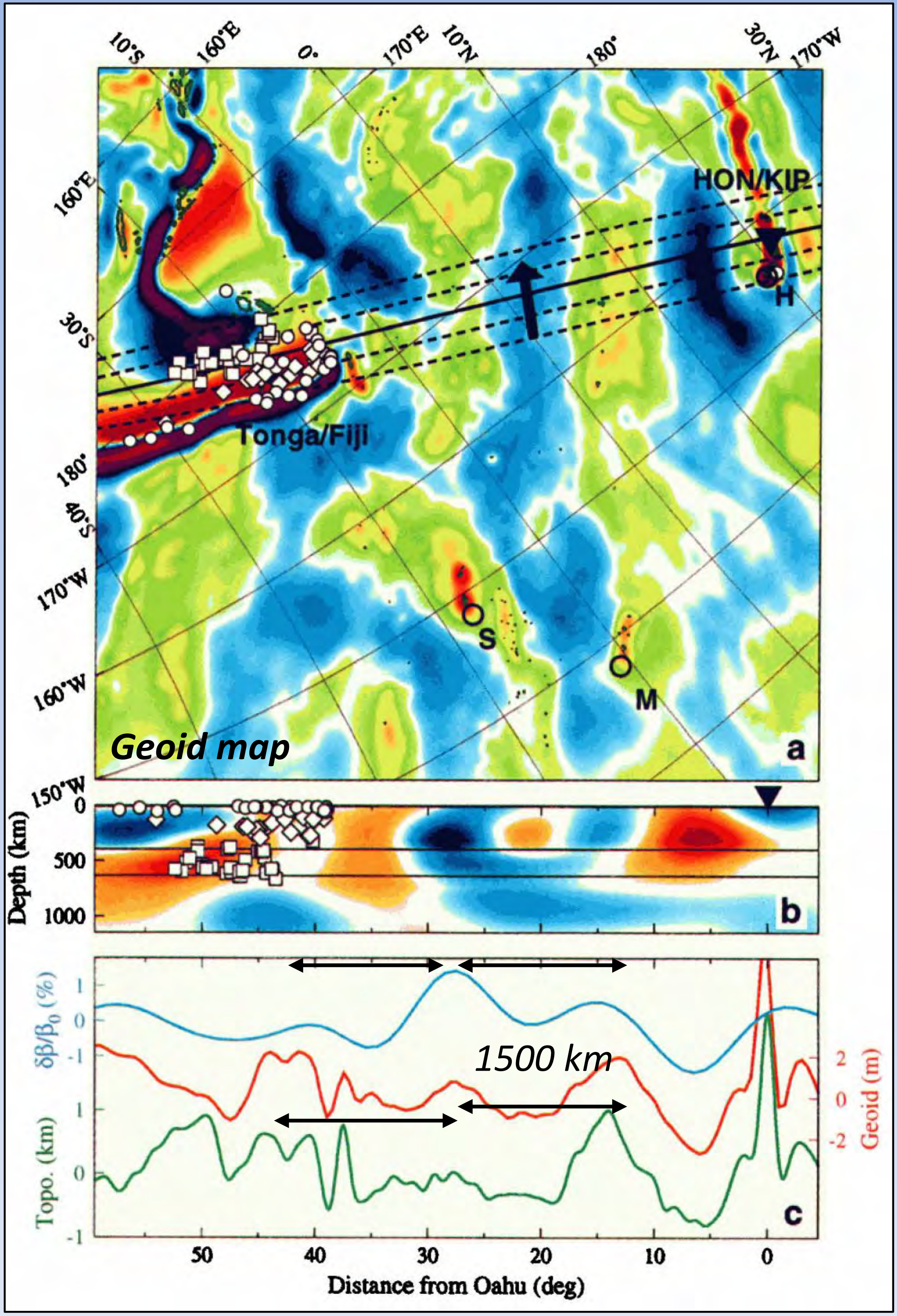

Katzman et al. (1998)

Dynamical modelling of the geodetic observations

Modelled Bouguer gravity and surface dynamic topography:

– Earth's response to an internal load, 4 internal interfaces: Moho, 410 and 660-km, CMB.

– newtonian attraction of the rolls thermal mass anomalies ($\Delta T = \pm$ 75 to 200 K)

– mass redistributions in a viscous, compressible Earth:
- dynamic topographies: mostly at the surface
- density variations in a compressible Earth

– 410/660 interfaces deflections: mostly due to the thermal anomalies, considering the olivine phase transitions.